A perspective on the Fe-based superconductors

TOPICAL REVIEW

A perspective on the Fe-based superconductors

John A Wilson

H H Wills Physics Laboratory, University of Bristol, Bristol BS8 1TL, UK

E-mail: john.a.wilson@bris.ac.uk

Abstract
FeSe is employed as reference material to elucidate the observed high T_c superconducting behaviour of the related layered iron pnictides. The structural and ensuing semimetallic band structural forms are here rather unusual, with the resulting ground state details extremely sensitive to the precise shape of the Fe–X coordination unit. The superconductivity is presented as coming from a combination of resonant valence bond and excitonic insulator physics, and incorporating boson–fermion degeneracy. Although sourced in a very different fashion, the latter leads to some similarities with the high temperature superconducting (HTSC) cuprates. The excitonic insulator behaviour sees spin density wave, charge density wave/periodic structural distortion, and superconductive instabilities all vie for ground state status. The conflict leads to a very sensitive and complex set of properties, frequently mirroring HTSC cuprate behaviour. The delicate balance between ground states is made particularly difficult to unravel by the micro-inhomogeneity of structural form which it can engender. It is pointed out that several other notable superconductors, layered in form, semimetallic with indirect overlap and possessing homopolar bonding, would look to fall into the same general category, β-ZrNCl and MgB_2 and the high pressure forms of several elements, like sulfur, phosphorus, lithium and calcium, being cases in point.

(Some figures in this article are in colour only in the electronic version)

Contents

1. Introduction

It had been my intent not to become involved with the pnictide superconductors, which were taken as a distraction from the hole-doped cuprate superconductors, and which it would appear are in another class, another league. However the pnictides are beginning to project certain lines of thought, detrimentally I believe, back into the cuprate problem. Moreover preconceptions concerning what is afoot in the pnictides seem to be taking many in altogether the wrong direction in that field too. Here I draw upon my long background [1–4] in addressing the full array of transition metal materials, often from a somewhat more chemically oriented perspective than the majority of solid state physicists, in order to (1) present the critical situation in play in the pnictide systems, (2) relate it to the different situation existing in the cuprates, and (3) indicate how it will generalize to a striking class of newly emergent superconductors, namely the semimetallic, homopolar bonded, low-dimensional polymorphs of the elements, among them iodine, phosphorus, sulfur, lithium, calcium, yttrium, etc, accessed under high pressures.

I have long discussed the mixed-valent HTSC cuprates in terms of negative-U effects (based on p^6d^{10} shell closure within a Cu(III) coordination unit), the superconductivity being then driven by boson–fermion resonant crossover. The touchstone to such behaviour lies with bulk disproportionation. Conversely, with the pnictides the corresponding bases are perceived as being resonant valence bond (RVB) behaviour and the excitonic insulator. As with the HTSC cuprates, the striking superconductive properties are once again viewed as arising in a resonant mixture of bosons and fermions, but this time gained under novel semimetallic governance.

In what follows

- section 2 surveys the chemical and structural setting of Mackinawite FeS and FeSe, emphasizing the control the unusual bisphenoidal coordination geometry exercises over the clash between the magnetic and superconductive behaviour exhibited here and in the related pnictides.
- Section 3 provides a closer look at the very profound effect that direct Fe–Fe bonding has upon the sequencing of the various d-states within the present $Z = 2$ structural setting.
- Section 4 makes an examination of the resulting semimetallic band structure and the critical role that correlation here has in arriving at an adequate description of the experimental findings.
- Section 5 looks at the intertwining of resonant valence bond and excitonic insulator physics in establishing high T_c superconductivity here. Exposition is made of the similarities and differences between what is occurring in the pnictides as against in the mixed-valent HTSC cuprates.

- Section 6 takes a detailed look at ten very different types of experimental work reported for the pnictides and interprets the results on the above basis.
- Section 7 examines how widely based adjustment to the chemical content of the unit cell facilitates a very sensitive and complex control over the interplay between the magnetism and the superconductivity observed with this group of materials.
- Section 8 points to the important role that the lattice exercises within the tripartite action precipitated by the excitonic insulator/RVB physics in play.
- Section 9 probes the form and origin of the electronic and structural inhomogeneities generated in the delicate balance between possible ground states for the present semimetallic systems.
- Section 10 suggests that the superconductivity at elevated temperatures met with in certain other low-dimensional, semimetallic materials that involve homopolar bonding, such as many non-metallic and metallic elements under high pressure, appears to partake of certain aspects of what is arising in the pnictides, as likewise do materials based on β-ZrNCl.
- Section 11 attempts to draw together all the many strands included in this survey and to restate the form of interpretation being offered for pnictide superconductivity, making contrast with what has been set out previously concerning cuprate HTSC behaviour.

2. A background to the pnictide materials

FeAs is a magnetic, metallic material, but it is an Fe(III) material, and the pnictide superconductors we are dealing with here are Fe(II). LnO·FeAs basically is a tetragonal layered form of FeAs fully intercalated by the monovalent cation, LnO$^+$. (N.B. the Ln atom sits on the outside of the LnO sandwich.) The uranyl $(UO_2)^{2+}$ and vanadyl $(VO)^{3+}$ cations are further, perhaps more familiar, examples of such oxycations, common for the more electropositive elements. The present $(LnO)^{1+}$ role [5] becomes explicit with the comparable system LiFeAs ($T_c = 21$ K) [6], and indeed BaFe$_2$As$_2$ [7] once written Ba$_{1/2}$·FeAs. (Note the latter under pressure becomes superconducting without any recourse to potassium doping [8].) Now one's frame of reference in contemplating the properties of NaTiO$_2$ is not Ti(IV) but Ti(III), and in the present case it is not Fe(III) but Fe(II). Accordingly it is to FeSe, not FeAs, that one is directed. It has by now become well publicized that tetragonal FeSe exhibits the same characteristic superconductive aspect to its behaviour, particularly under pressure [9], as that found in the more widely researched pnictides. Other crystallographic forms of FeSe do not display anything comparable, and hence the key to the behaviour has to lie with the detailed crystal structure and ensuing band structure.

The highly unusual nature of the tetragonal Mackinawite form of FeS has long been recognized [10, 2]. FeS normally is encountered in hexagonal nickel arsenide form (Pyrrhotite, toward which Mackinawite is unstable above 150 °C). In Pyrrhotite the iron ions are octahedrally coordinated and

show high-spin (h.s.) behaviour to produce an $S = 2$ magnetic metallic material [11]. At lower temperature in stoichiometric samples of pyrrhotite a basal trimerization occurs, seen in the mineral form Troilite [12]. FeS finally can be secured in tetrahedrally coordinated zincblende form [13]. With the latter there exist no short Fe–Fe distances and this polymorph manages to retain Mott-insulating character, much as in octahedrally coordinated h.s. d^6 FeO. Remember, though, now in tetrahedral coordination—at least given a regular tetrahedron in apical orientation—the ten d-states will experience local symmetry splitting 4-and-6 (e/t_2), not the 6-and-4 t_{2g}/e_g division so familiar with octahedral coordination [14].

In the Mackinawite form of FeS the structure displays several important differences from its Mott-insulating zincblende polymorph. The tetrahedra now share edges rather than corners [10]. That brings about a layered tetragonal 2D net rather than a 3D one, and one most importantly containing a much shorter nearest-neighbour Fe–Fe distance (2.60 Å versus 3.83 Å). The tetrahedra no longer are constrained by the adopted structure to be ideal in form (i.e. of uniform interbond angle 109° 28′), and they find themselves not in apical orientation either. The tetrahedra in this uncommon tetragonal structure form two mutually perpendicular, basal strings of bisphenoids (crossed wedges) with the crystallographic z axis running between opposed edge-centring locations. All the iron atoms reside at crystallographically equivalent sites (point symmetry $\bar{4}2m$), the unit cell holding two such atoms (i.e. $Z = 2$). The space group is No. 129, non-symmorphic D_{4h}^7 ($P4/nmm$). This implies for the band structure the presence of twice as many bands as with the $Z = 1$ zincblende polymorph (e.g. 6 sulfur-based p-bands, not 3)—a feature shortly to prove key in understanding how Mackinawite FeS ends up a semiconductor.

Now Mackinawite FeS is not the only semiconducting sulfide of Fe(II). The best known of all iron sulfides is iron pyrites (see figure 7 in [1]). FeS₂ derives from rocksalt FeO when all the O^{2-} ions are replaced by $(S_2)^{2-}$ pseudo-halogen dimers. These dimer ions align systematically along the four different body diagonals of the cubic structure reducing the space group from O_h^5 ($Fmmm$) to T_h^6 ($Pa3$). In the rocksalt structure the octahedra shared all their edges, but now in the pyrite structure the S_2^{2-} units spring the octahedra apart so as to share corners only. The outcome is a $Z = 1$ basis with fcc rocksalt, but with the pyrite-structured material a $Z = 4$ basis. Transfer from the oxide to the sulfide moreover tips the balance from a high-spin to a low-spin state; i.e. the increased covalence (p/d hybridization) of the sulfide causes crystal field/molecular orbital effects to become dominant over Hund's rule spin coupling. One can in fact follow such transfer under pressure in hexagonal FeS [15]. Crossover occurs quite rapidly as a result of the sharp reduction in bond length (and hence cell volume) accompanying conversion of antibonding $dp\sigma^*$ (here e_g) electrons into non-bonding $dp\pi$ (here t_{2g}) electrons. With d^6 FeS₂ the end product is a minimum semiconductive band gap of 0.9 eV between the t_{2g} and e_g manifolds [16]. Since in FeS₂ $Z = 4$, there are going to exist $3 \times 4 = 12$ of the former subbands and $2 \times 4 = 8$ of the latter in the developing horizontal spaghetti.

With FeS₂ and the rest of the 3d pyrite disulfides, (d^7) e_g^1 CoS₂, (d^8) e_g^2 NiS₂, (d^9) e_g^3 CuS₂, and (d^{10}) e_g^4 ZnS₂, great simplicity is conferred upon their properties by the cations remaining tethered to the fcc sublattice. This is what makes NiS₂ the archetypal material for studying the Mott transition [17, 1, 4], as against a corundum-structured material like d^2 V₂O₃, where the cations are free to shift along the c-axis—indeed in d^1 Ti₂O₃ to dimerize. In the alternative semiconducting, orthorhombic, Marcasite polymorph of FeS₂ (see figures 8 and 9 in [1]) the octahedra there now form edge-sharing strings. The capacity then for cation dimerization becomes realized under the appropriate t_{2g}^5 circumstance of arsenopyrite Fe(AsSe), this negated upon returning to t_{2g}^6 and Co(AsSe). When dealing with all these materials it is essential always to appreciate the functionality of the component units; witness Fe₂(P₂S₆) is a water-soluble thiophosphite [18], not a phospho-sulfide.

One is required now to address how Mackinawite FeS manages to be a semiconductor at d^6 when holding *tetrahedral*, not octahedral coordination. This non-metallic outcome is accomplished without any crystallographic distortion from the simple layered tetragonal structure, one shared by Li(OH)—and in anti-site form by PbO. A low-spin non-magnetic condition immediately is made evident from the single-spiked Mössbauer spectrum [10, 19]. That however does not simply imply core diamagnetism, as with a standard non-T.M. semiconductor. A strong, countering, almost temperature-independent van Vleck paramagnetic term is found here [20], much as in FeS₂ [21]. One accepts non-metallic FeS₂ to be a semiconductor and not a Mott insulator since it can readily be doped both n-type and p-type to yield material of moderately high mobility ($\geqslant 1$ cm² V⁻¹ s⁻¹) [1]. Such might not be true of the 3d⁶ oxide Co₂O₃ [22] (l.s. analogue of corundum-structured 4d⁶ Rh₂O₃ and perovskite-structured LaRhO₃ [23]), but it appears the case for tetragonal FeS. By FeSe there is no doubting its delocalized credentials, by then there occurring significant semimetallic d–d overlap under the augmented covalent p/d hybridization. Nonetheless a more customary magnetism emerges in 'FeSe' when one allows the stoichiometry of the system to deviate from strictly 1:1 [24]. Superconductivity in contrast occurs in FeSe under standard conditions right at stoichiometry [25] with $T_c = 9$ K. From this value T_c proceeds to climb in two stages to a maximum of 36 K [9] under a hydrostatic pressure of 8 GPa (80 kB), before declining again. Clearly the superconductivity showing up here is highly sensitive in kind to the detailed adjustment of the crystallographic free parameter, u_z, detailing the precise location of the Se atoms along the c-axis (see figure 2 below); i.e. the superconductivity is highly dependent upon the precise shape of the Fe–Se coordination unit.

In the pure selenide the bisphenoid is slightly elongated along the c-axis [24a, 26], and, for a layer compound such as the present, *hydrostatic* pressure will actually increase that form of deformation, as the softer van der Waals (vdW) gap region permits the more rigid Fe–Se framework of bonds to concertina into it. Comparable shape sensitivity is apparent with the LnOFeAs family of superconductors, for which the
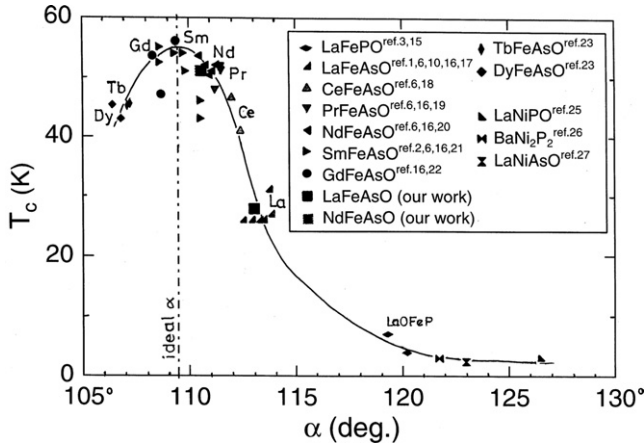
Figure 1. A plot of bond splay angle, α, within the bisphenoidal Fe coordination unit versus achievable T_c, for a wide range of iron arsenides and phosphides. The plot shows the maximum value T_c^{max} attainable superconductors (at 1 atmos) with each system included, and it features the sharp global maximum of 56 K realized within the SmOFeAs system as α transits the value of 109° 28′ for a regular tetrahedron. Note the progression across this peak traced out by the rare-earth series in 1111-Ln arsenides, corresponding to growing basally directed chemical pressure upon the Fe–X sandwich from right (La) to left (Dy). The plot is taken from Lee *et al* [27] (reproduced here with permission of *J. Phys. Soc. Japan*: copyright 2008). Note additionally the more recent results—1111-Ho [27b]; -Er $T_c = 36$ K; 33 K. SrFe$_2$As$_2$ [8a, 146]; $\alpha = xxx°$, $T_c = 6$–26 K. LiFeAs [6]; $\alpha = 103°$, $T_c = 21$ K. FeSe (1 Atm.) [26b]; $\alpha = 105°$, $T_c = 11$ K.

maximum attainable T_c peaks across the lanthanide sequence at Sm, as is seen in figure 1 [27]. In the latter '1111'-materials, *basally directed* chemical stress becomes transmitted from the contracting LnO layers into the FeAs layers as the LnO ionic unit steadily is diminished in size down through the f^0 to f^{14} sequence. The stress becomes appropriate within this family optimally to tune T_c to 54 K at the case of f^5 Sm(III). And the telling empirical observation here regarding what this tuning amounts to is that it imports to the bisphenoidal FeAs coordination unit ideal tetrahedral geometry: that is the interbond angle As–Fe–As across the z axis, α, to be referred to as the bond splay angle, takes on the ideal tetrahedral value of 109° 28′. (Note $\alpha = 180°$–2θ, where $\theta = \tan^{-1}(u \cdot c / \frac{1}{2}a)$ see figure 2 below.) Such ideality of local form is not one enforced by the crystal space group, but one that when attained critically influences the local molecular orbital energies and interactions. The consequences feed through automatically into the detailed band structure to govern the material's electronic properties. Under the structurally resonant conditions, SmOFeAs (as with Mackinawite itself) takes up a non-magnetic, Fe-singlet condition of the same key form, in evidence once again in the Mössbauer and NMR data [28]. Note from figure 1 many of the other materials presently being discussed in connection with pnictide superconductivity, like LaOFeP [29, 30], lie with α far removed from ideality, and these systems exhibit varying degrees of resurgent magnetic behaviour and then (much) lower superconducting T_cs.

3. From molecular orbitals to a band structure for Mackinawite FeS

Let us first examine in greater detail the form of the Mackinawite structure. Figure 2(a) shows an ideal tetrahedron in bisphenoidal orientation, with x, y and z axes attached as appropriate to the tetragonal structure. The four triangular faces all are inclined and at mid-height, where the iron lies, they define a horizontal, square intersect, featuring in the basal projection of figure 2(b). In tetragonal FeS these tetrahedral coordination units share all four inclined edges to produce a structure rather like a waffle, where square pyramidal pits just extend through the S–Fe–S layering, the pits on the reverse side then being displaced by $(\frac{1}{2}, \frac{1}{2})$ from those on the top. The small Fe ions fill all the bisphenoidal interstices between the S layers to yield a square-centred array and the 1:1 stoichiometry. In FeS the waffles sit directly above one another. Figures 2(c) and (d) illustrate the situation in side elevation and in plan respectively.

If the van der Waals (vdW) gaps between successive sandwiches were to hold exactly the same interlayer S–S separation as that within the S–Fe–S sandwiches, the S layers would sit at $z = \frac{1}{4}$ and $\frac{3}{4}$. However the vdW region is much reduced in thickness. While $u_z(S)$ indeed proves to be somewhat bigger than $\frac{1}{4}$, this does not immediately imply that the FeS coordination units themselves are automatically stretched along z compared with ideal geometry. Upon using the above quoted formula one discovers that in fact α (the intra-sulfur-sheet bond splay angle) is remarkably close there to the ideal value of 109.45°. With the selenide, for which the atomic positions are better refined ($u_z = 0.267$), α proves to lie appreciably below ideal at 104.1°, meaning the coordination unit now indeed is elongated [24a]. We throughout shall employ angle α to monitor deformation of the tetrahedron, whether as presently or in the related structures of LnOFeAs, BaFe$_2$As$_2$, etc (for which α most frequently is greater than ideal, as may be seen from figure 1). Given the current layer compound setting, as was indicated above, the initial effect of applied *hydrostatic* pressure [9] is to push up coordination unit elongation, decreasing angle α. The slight (orthorhombic) quadrupolar splitting of the Mössbauer singlet found in FeSe at lower pressure actually vanishes in this process [26c]—a matter of much interest later in section 8.

Although the Fe ions within a layer sit on a square-centred array, the FeS sandwich as a whole does not possess face-centred symmetry. Each sandwich of the primitive tetragonal cell contains two Fe, in bisphenoids possessing 90° relative twist (the two otherwise being physically equivalent). This latter twist means the horizontal mirror plane of the relevant space group, $P4/nmm$, is not a simple mirror but a glide plane associated with translation $(\frac{1}{2}, \frac{1}{2})$. A whole series of vertical glide planes (in 45° orientation) along with horizontal screw diads (both in axial and 45° orientation) result, as set out in the International Crystallographic Tables (vol. 1; group # 129). We have portrayed above in figure 2 what might be termed the natural setting for our material, positioning a Fe atom at the cell corner, and this fortunately proves (in the present case) to be a crystallographically acceptable choice (known as 'setting
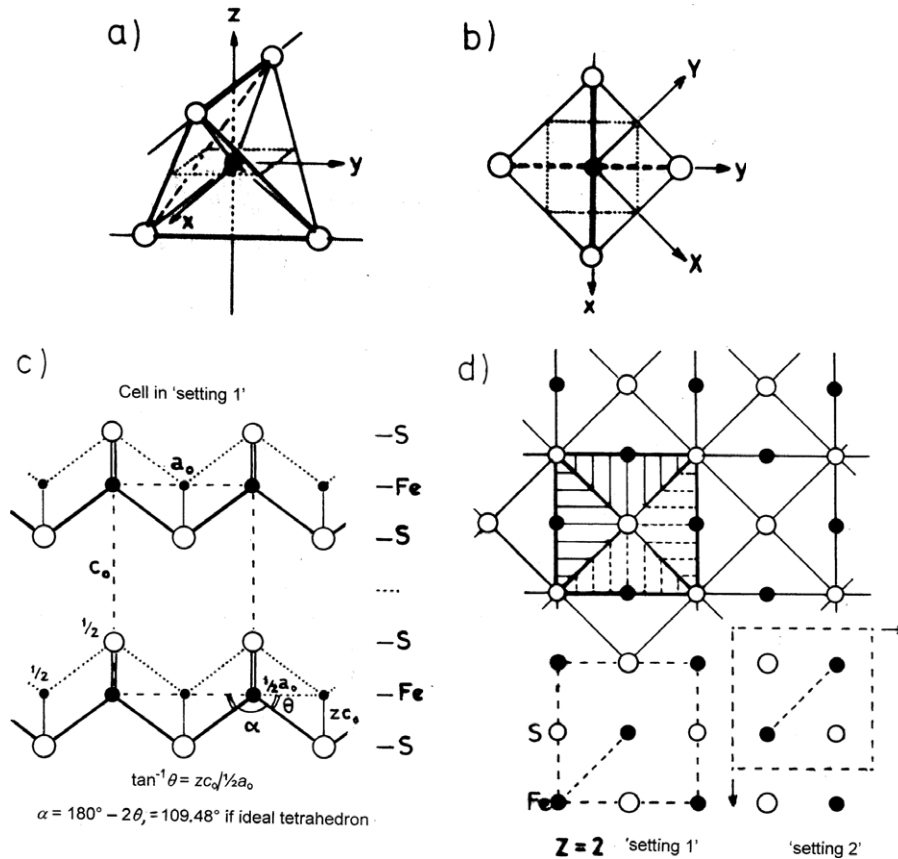
Figure 2. (a) Bisphenoidal orientation of tetrahedron present in Mackinawite FeS. There occurs here slight elongation along z as compared with a regular tetrahedron. The Fe atom resides halfway between the upper and lower crossed edges of the coordination unit. The latter run parallel to the x, y axes of the tetragonal cell. The units share all four remaining edges to build a layer structure. (b) Basal projection of the bisphenoid unit. The inner, dotted square marks the horizontal section through the central Fe site, and the X, Y axes shown form the natural symmetry axes of the unit. Directed to the mid-points of the inclined tetrahedral edges (and beyond in the full structure to the n.n. Fe sites) they run at 45° to the crystallographic axes x, y for the Mackinawite structure. (c) Side elevation of the layered Mackinawite form of FeS, in which the FeS sandwiches sit directly above each other across a somewhat contracted vdW gap. Bond splay angle α monitors the level of deformation of the tetrahedra from being regular (109° 28′). N.B. $\sin(\alpha/2) = \frac{1}{2}a_o/B$ and $\tan(\alpha/2) = \frac{1}{2}a_o/U$, where B is the FeS bond length and $U = u_z(S).c_o$. (In FeS $a_o = 3.678$ Å, $c_o = 5.039$ Å, and for $u_z = 0.258$, α would be ideal. In FeSe $u_z = 0.268$ making $\alpha = 104°$ [24a].) (d) Single FeS sandwich of Mackinawite structure in plan. The form of the sandwich is like a waffle with square pyramidal pits that just penetrate its thickness. The pits on the reverse side are staggered by $(\frac{1}{2}, \frac{1}{2})$. The $Z = 2$ crystallographic unit cell, tetragonal space group D_{4h}^7, P/nmm, #129, requires that in 'first setting' the Fe atoms lie at the cell origin ($\bar{4}m2$). The nearest-neighbour Fe distance between the atom at the corner of the f.c. Fe planar array and that at its centre is just 2.60 Å. The alternative 'second setting' sees a transfer of the cell origin to the centre of inversion at $(\frac{\bar{1}}{4}, \frac{1}{4})$.

1'). However a cell choice displaced from the above by $(\frac{1}{4}, \frac{1}{4})$ (what is known as 'setting 2') perhaps better exposes the equivalent disposition of the two Fe atoms within the $Z = 2$ structure. The above space group is going automatically to bring about ubiquitous band degeneracy in certain parts of the band structure, specifically within the vertical faces of the Brillouin zone.

Before examining the band structure itself it is beneficial for this material—one still quite close to the Mott transition— to establish a molecular orbital picture of those strong local ingredients set to proceed into the overall crystal potential. One crucial feature to appreciate here is that the natural local symmetry axes of the tetrahedra are not those of the crystal structure x, y, z, introduced in figure 2, but X, Y, Z, rotated from the former set by 45° in the basal plane. The non-bonding orbitals become labelled then d_{XY} and d_{Z^2}, each

pointing towards the edge mid-points of the tetrahedron. d_{XY} accordingly aligns in the directions of the four nearest-neighbour Fe sites within the crystal lattice. These neighbour Fe sites fall so close (at only 2.6 Å in the sulfide) that there will arise significant $dd\pi/\pi^*$ basal interaction in the band deriving from this source (with very little k_z dispersion). By contrast d_{Z^2} because of its moderate δ-type overlap with the p_z orbitals of the sulfur atoms will display some k_z dispersion, but now with rather little basal dispersion. Of the *anti* bonding $pd\sigma^*$ states, the one parented by $d_{X^2-Y^2}$ engages relatively weakly with all four sulfur atoms and will be least strongly elevated, while the remaining pair of states d_{XZ} and d_{YZ}, which rise more strongly in σ^* fashion from interaction with the sulfur sublattice, will in addition experience appreciable bonding/antibonding π interaction with their n.n. iron atoms (though not quite as much as d_{XY}).
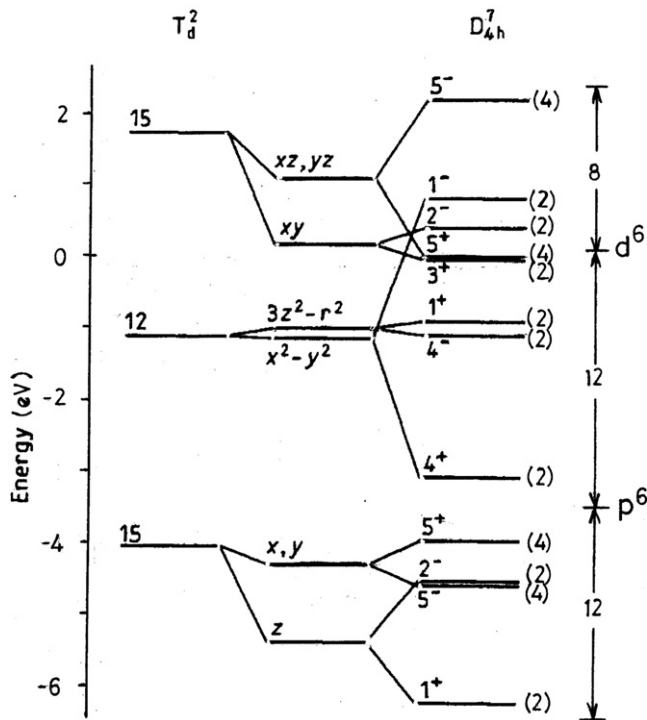
Figure 3. Molecular orbital level scheme for Mackinawite FeS, covering the S 3p- and Fe 3d-derived states, this directly bearing on the band structure at the Γ point. The figure indicates how the levels for an isolated tetrahedral coordination unit, sphenoidally oriented in the crystal field, become first modified from the customary levels of the zincblende form and then further much modified in the current $Z = 2$ structure under the very strong direct Fe–Fe interaction (separation just 2.60 Å). The parentage of the states is indicated in the centre of the figure, whilst the symbols to the right give the representations appropriate to space group D_{4h}^7, to appear on the band structure below. The numbers in brackets mark the various state electron capacities. With the present complement of 12 d electrons for the $Z = 2$ Fe(II) condition, the closely spaced pair of states 3^+ and 5^+ which issue from d_{xy} and d_{xz}, d_{yz} respectively will constitute the top of the V.B. Note both the latter are $pd\sigma^*$ states driven downwards below E_F by the Fe–Fe bonding. This addition to the V.B. is partially countered by analogous strong elevation above E_F of the $dd\pi^*$ antibonding partner issuing from $d_{x^2-y^2}$, so fixing the energy gap for d^6 FeS to be between the π and π^* states which emerge from d_{xy}. Note above we are using state designations relative to the crystallographic axes x, y, not the coordination unit axes X, Y. Figure based on that of Welz and Rosenberg [33]: (copyright: IOP, 1987). The energy scale has been transcribed from Rydbergs to eV and the zero level shifted very slightly to coincide with the top of the valence band.

In figure 3 we present the evaluated $Z = 2$ pattern of M.O. levels; this duly will go forward to dictate Γ-point ordering in the full band structure. The numbers in brackets here mark the state electron complements. The designations applied to the states relate, note, now to the crystallographic axes and *not* to the local axes for the coordination unit introduced above. Behind this transcription will lie appropriately symmetrized state mixing. For FeS one should expect the main valence band, largely parented by the six sulfur 3p-states, to lie fully separated off from the d-dominated states above. Straightaway from figure 3 one is able to recognize the remarkableness of a semiconducting
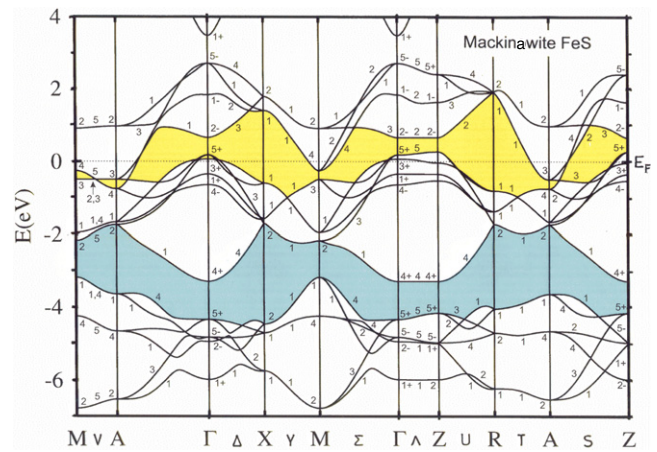

Figure 4. (Coloured online) LMTO band structure for tetragonal FeS obtained in the A(tomic) S(phere) A(pproximation) and using the L(ocal) D(ensity) A(pproximation) to treat correlation and exchange. The figure comes from the paper by Subedi *et al* [31]; (copyright: APS 2008). Shading has been added to indicate the extent of direct gapping between the p- and d-bands, and similarly with regard to the intra-d-band gapping about E_F under the $Z = 2$ cell's 12-electron complement at Fe(II) d^6 loading. The figure has been amplified to show the symmetry representations at the special points in the zone, this information extracted from the paper by Welz and Rosenberg [33]. Note the compulsory band degeneracy arising throughout the cuts XM, MA and AR due to the presence of the horizontal glide plane.

(or even low-overlap semimetallic) end product with our current complement of twelve 'd' electrons. It will call for more than simply the weak splitting of the xy level within the $Z = 2$ band structure, in view of the simultaneous strong movements of the topmost x^2-y^2 ($dd\pi^*$) state upwards and of the lowermost ($dd\pi$) level deriving from the xz/yz doublet downwards. Responsibility for a very low density-of-states outcome at E_F has in some measure to stand as a consequence of the relatively low symmetry of the space group. With representation characters being there restricted over large sections of the zone to unity, such bands are forbidden to cross but necessarily will hybridize and gap. The bands in addition become more readily able to acquire compatible tie-in's in any given energy range. Nonetheless it remains remarkable that the bottommost states from σ^*xy, as again with the degenerate π-bonding pair from yz and zx, can manage throughout to pick up dispersion to *lower* energy, whilst the elevated x^2-y^2 π^*-state acquires dispersion to *higher* energy, all in a manner such as facilitate the slotting through of a gap embracing precisely the 12 electrons in hand. The role of spin and charge correlation in securing this outcome will need to be addressed further.

Figure 4 provides, without offering much insight into the above matters, a modern LAPW band structure for tetragonal FeS [31]. The shading added here highlights the extensive direct gapping suited to accommodation of our 12 electrons in a low DOS fashion. Whether in reality with the sulfide there is very slight semimetallic overlap as here, or whether a more refined treatment of the correlation will secure a true semiconducting gap is a problem for later. Where semimetallic overlap definitely is encountered is in the selenide due to
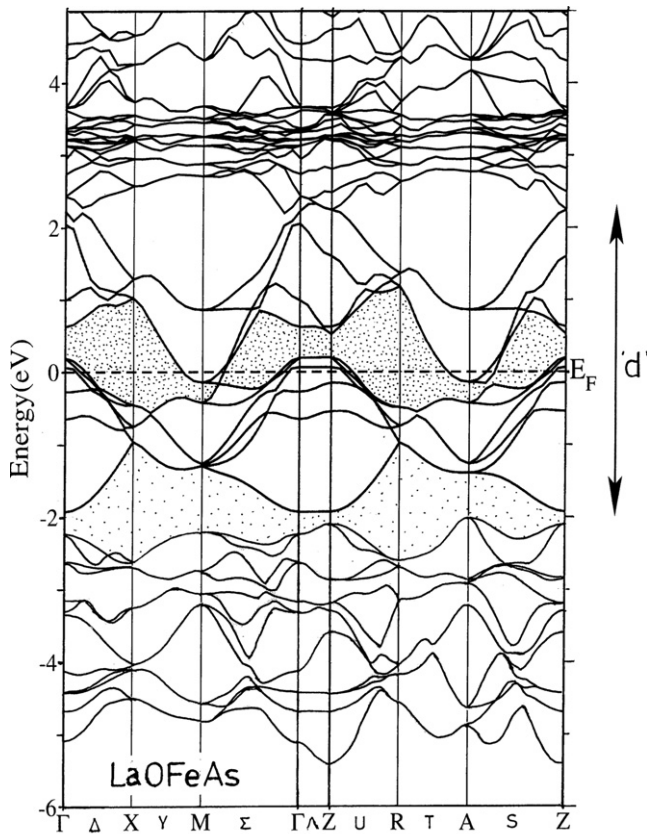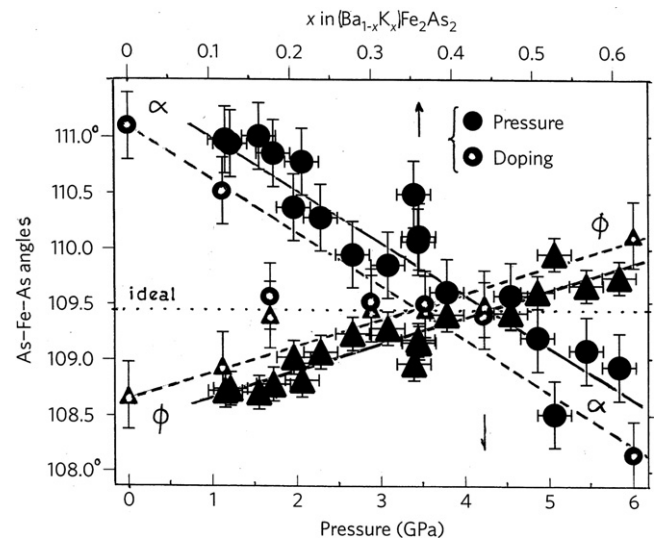
Figure 5. Band structure for LaOFeAs obtained by Vildosola *et al* [35] using LAPW method and following the WIEN2k routine within LDA. The band structure is strikingly similar to that of figure 4 for tetragonal FeS. The shading about E_F makes evident the small indirect overlap between the VB maximum at Γ and CB minimum at M, the cell corner. The widths of the occupied and unoccupied sections of the d-band are here somewhat over-stated, making this overlap too large. The calculation enfolds the *experimentally* derived value for α of 114.6°. (Reproduced with permission of APS: copyright 2008.)

Figure 6. Key result from Kimber *et al* [36] for the BaFe$_2$As$_2$ system showing the identical behaviour of the structure under hydrostatic pressure and under K-doping. Both agencies secure, following elimination of the orthorhombic distortion, a growth and then decline of T_c over a maximum reached in the pressure sweep at 4 GPa and in the doping sweep at 35% K. The plot reveals that under *both* procedures the maximum T_c value materializes precisely as the tetrahedron passes through the *regularized* interbond angle, 109.44°. (Reproduced with permission of MacMillan press: copyright 2009).

the now greater degree of p/d hybridization, but remarkably the carrier pockets observed experimentally, even with heavy tellurium admixture [32], still appear quite small.

Before closing this section it has to be noted that the above band structure from Subedi *et al* [31] in fact is not the first to be derived for Mackinawite. On scanning the literature an earlier calculation from Welz and Rosenberg [33] was uncovered, made in the period just prior to HTSC and well before current interest in the pnictide and related superconductors. Their paper ties in nicely much of the early literature on the Mackinawite problem. The method they employ is SCLMTO, pursued within the atomic sphere and local density approximations. In its detailed form the product matches remarkably closely the more recent version, thereby serving to emphasize the still rather localized nature of FeS. With tetrahedrally coordinated FeS it is expected from the overview reached spectroscopically and magnetically in [2] that Hubbard U will here be someway below the overall d-bandwidth, and probably in the range of 1.5–2 eV.

One of the benefits of the above LMTO calculation is that it provides valuable information regarding the symmetry

representations for the bands at the various special points and along the special lines of the B.Z. That information has been transcribed now from [33] onto the bands of figure 4. The representation labels used follow the notation introduced by Bradley and Cracknell in their extensive group theoretical review [34]. Take note of the universal band degeneracies within the vertical faces of the B.Z. (along XM, MA and AR) instigated by the glide plane in $P4/nmm$.

4. Pnictide band structures and the matter of coordination unit shape tuning for T_c optimization

The band structure for LaO·FeAs is in general form strikingly similar to that of tetragonal FeSe as can be seen from figure 5. This particular calculation comes from Vildosola *et al* [35] and it was generated using the full-potential APW and local orbitals method, and implemented under the WIEN2K code within the LDA correlation and exchange approximation. The band structural detail in close proximity to E_F emerges, as anticipated, as being supersensitive to surprisingly small changes in $u(z)$ and angle α. These coordination unit shape changes prove, as evidenced above in figure 1, to be critical for the magnetic/superconducting outcome acquired in any given member of the family. The closer α comes to 109° 28′, the more favourable conditions are toward superconductivity and to elevated T_c. The situation very graphically is portrayed in figure 6 for the BaFe$_2$As$_2$ system. Since the latter compound suffers a small orthorhombic distortion at low temperatures which is detrimental to superconductivity, this material customarily is encountered doped with potassium
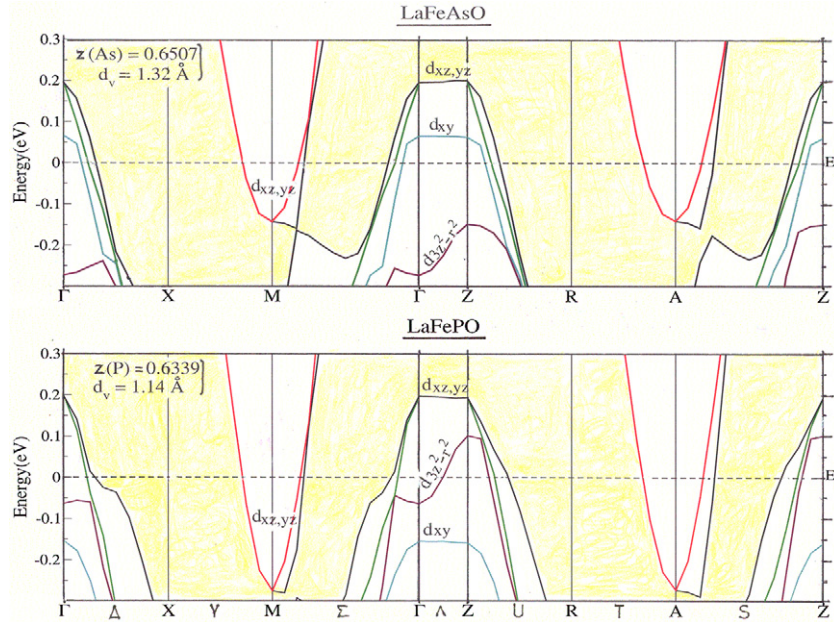
Figure 7. A blow-up of figure 5 for LaOFeAs ($\alpha = 114.6°$) in the vicinity of E_F, for comparison with the corresponding result for LaOFeP ($\alpha = 120.2°$). The semimetallic overlap is smaller in the arsenide and the d_{xy} and d_{xz}, d_{yz} states in the Γ pocket have come closer to triple degeneracy as α is shifted toward ideality. (From Vildosola *et al* [35]; reproduced with permission of APS.)

so as to suppress the lattice distortion and grant access to the superconducting state. It is found that there exists an optimum doping level in the latter procedure. With $BaFe_2As_2$ a comparable outcome may, as already noted, also be realized under pressure. A very telling discovery tying the above two eventualities together is that made by Kimber *et al* [36]. Their key observation, reproduced now with some clarification in figure 6, is that, when pursuing *either* procedure, angles α and ϕ come to assume tetrahedrally ideal form exactly as T_c optimizes. To understand what is going on here one needs to return to the band structure to see just what such shape ideality crossover actually secures.

Drawing once more on the work of Vildosola *et al* [35], figure 7 presents the detailed form of the band structure in the vicinity of E_F for two contrasting 1111-materials, LaOFeAs ($\alpha = 113.5°$; $T_c^{opt} \sim 26$ K) and LaOFeP ($\alpha = 119°$; $T_c^{opt} \sim 6$ K). The bands have here been labelled with the dominant state parentage symbols identified in figure 3. Examination of these two differently detailed band structures uncovers three changes of import existing between them. On passing from the phosphide to the arsenide (and to higher T_c), one observes (a) a considerably deeper location at Γ for d_{z^2}, this lying now well below E_F, (b) a considerably lowered energy at Γ as well for the (hole-bearing) doublet d_{xz}, d_{yz} relative to the conduction band minimum at M, (c) a d_{xy} position not greatly altered with reference to the latter point, this meaning doublet d_{xz}, d_{yz} has been brought in the arsenide to a level much closer to degeneracy with the d_{xy} state. The above changes are perceived to issue from the following causes: (a) comes from a reduced broadening of the d_{z^2} band in the arsenide, which in turn comes from reduction in d_{z^2}/p_z overlap as the distance to the arsenide layer recedes under the augmented sandwich height with the fall in α: (b) is an outcome of the smaller angle α leading,

moreover, to greater state separation between the $dd\pi$ and π^* states that occur within the d_{xz} and d_{yz}-derived set of states, due to the now stronger n.n. Fe interaction: (c) the latter change forces the inter-Fe-site π-bonded doublet of states (d_{xz}, d_{yz}) into a closer proximity with the (lower) d_{xy} state—which recall from figure 3 is itself an inter-Fe-site bonded state. The above advance toward full degeneracy of the d_{xz}, d_{yz} and d_{zx} states would look to be what is procured as SmOFeAs approaches shape ideality.

Now why should this coincidence have such profound influence upon the superconductivity attained? An important feature to register here is that the three key states figuring above all are spin-paired states, each entailing secondary M–M bonding interaction between near-neighbour Fe sites. They facilitate a prime example of resonant spin-pair (RVB) coupling, sustained for as long as the tetragonal lattice symmetry is retained. An undistorted environment expresses here the widely based covalent hybridization, often further assisted by disorder and the metallicity coming with doping. Breaking this structural symmetry through orthorhombic distortion sees the close degeneracy between the above three orbitals significantly impaired, and this can encourage local moment growth and ordering, always detrimental to superconductivity.

The occurrence of spin coupling in RVB fashion still demands a quite high degree of correlation, and such is precisely the area in which the current calculations are patently somewhat defective. As can be seen from figure 5, the overall d-band width that the APW-LDA routine prescribes for LnOFeAs is 4 eV. Given that in this material U is estimated to be ~ 1.5–2 eV, it is evident the as-calculated bandwidth is overstating reality by roughly a third. Such renormalization of the calculated bandwidth under more

elaborate treatment of local correlation effects than is afforded by the LDA approximation is strongly supported both by ARPES and dHVA/SdH (de Haas–van Alphen/Shubnikov– de Haas) experimentation. The photoemission results of Li *et al* [37] for LaOFeP would suggest an actual overall d-band width of only around 2.5 eV. The quantitative support dHVA provides in this direction [29] comes in the form of deduced band masses enhanced roughly twofold as compared with the corresponding masses gained from the band calculations. To achieve any match between the areal dHVA data and calculation has necessitated slight but significant mutual adjustment of the locations of the occupied and unoccupied bands about E_F. Their relative movement lies in the direction of shrinking all the carrier pocket sizes by diminishing semimetallic overlap, the electron band being shifted up, the hole band shifted down each by around 50 meV. In the main these data come, it should be pointed out, from material standing still quite some way from having α right at shape ideality. This is due not only to lack of suitable crystals, say for SmOFeAs, but also because in the dHVA/SdH work if T_c is high, then H_{c2} is high. Accordingly it no longer is possible to sense the normal state given the size of fields available (one requires H to be at least in excess of H_{irr}, i.e. running up beyond 30 T).

Now with conventional superconductors, and following the MacMillan and Dynes/Eliashberg approach (see Kresin and Wolf [38]), one customarily for high T_c within the BCS scenario looks towards a high density-of-states at E_F in conjunction with a strong electron–phonon coupling parameter, λ. In the present case neither of these are forthcoming (for analysis of this latter see Boeri *et al* [39]). On the contrary we are afforded prime manifestation of the non-conventional nature of the present superconductors. The current data for shape-optimized pnictides positions them plumb on the Uemura plot [40] for unconventional superconductors—a plot embracing the organic superconductors, the Bucky Ball superconductors, β-HfNCl, and above all the cuprate HTSC superconductors.

5. A perspective of the HTSC mechanism in FeSe and the iron pnictides that avoids over-eager appeal to spin fluctuations

The picture that we shall pursue below then is essentially the following. In FeSe and its ternary and quaternary analogues (figure 8) the unusual crystal structure inserts into the band structure a deep, rather narrow, density-of-states minimum at d^6. Strong residual correlation effects in the materials— ones not grossly removed from the Mott transition—secure an enhancement of that minimum, to a point where in FeS a semiconducting outcome can just be reached. This correlation effect can be expressed in terms of RVB spin-pair coupling, highly suited to the prevailing situation by virtue of the crystal structure holding two Fe atoms per unit cell, close in separation and in regular, face-centred square, layered setting. As long as the crystal structure holds and does not yield to symmetry distortion, the regular RVB bonding steadily establishes a low susceptibility, paramagnetic environment [41]. The then much constrained spin-flip pair-breaking constitutes a major asset
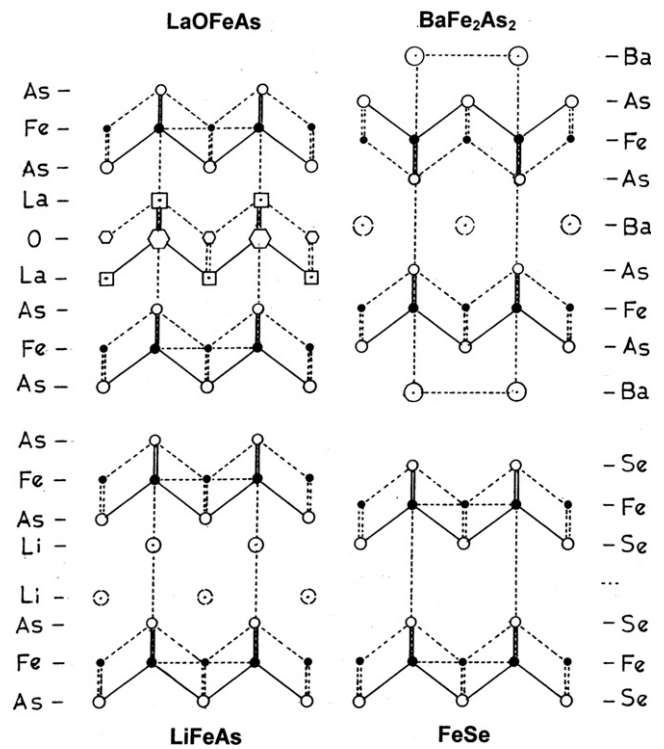
Figure 8. Side elevations, approximately to scale, of the tetragonal FeSe, LiFeAs, LaOFeAs (all in 'first setting') and BaFe$_2$As$_2$ $Z = 2$ unit cells. LaOFeAs (1111), $P4/nmm$, $a = 4.03$ Å, $c = 8.74$ Å; LiFeAs (111), $P4/nmm$, $a = 3.77$ Å, $c = 6.36$ Å; BaFe$_2$As$_2$ (122), $I4/mmm$, $a = 3.96$ Å, $c = 13.02$ Å; FeSe (11), $P4/nmm$, $a = 3.77$ Å, $c = 5.52$ Å.

toward the development of superconductivity. With regard however to conventional superconductivity, we pointedly are not in a promising situation since the density of states is very low and the material does not lend itself to strong electron–phonon coupling. Also, as layer compounds, their Debye temperatures are very low too ($\sim$250 K). What the systems do have running in their favour, however, is that the semimetallic overlap is associated with an indirect gap. (In this they are distinct, say, from the A15 superconductors like V$_3$Si.) With indirect overlap, there emerges for the semimetal a susceptibility to electronic instability with wavevector separating the overlapping electron and hole pockets.

In accord with the excitonic insulator treatment for this form of incipient instability [42], the system is prone either to a spin density wave, a charge density wave, or a superconducting instability, or all three, as appropriate to the individual circumstance. Charge and spin density waves ordinarily are addressed in terms of extensive and effective Fermi surface 'nesting', examples being Cr and 1T-TaS$_2$ [43]. However with the excitonic insulator situation the Fermi volume is rapidly approaching zero as the gap-bounding bands withdraw their overlap. For the pnictides it actually has become very apparent that the quality of geometrical nesting is not particularly good [29], especially where α remains at a distance from ideality (i.e. from the degeneracy between d$_{xy}$ and d$_{xz}$, d$_{yz}$), and/or the system has been 'doped', so destroying equality between the number of holes and electrons.

In an excitonic insulator situation one should not look to action of quite the same form as under more extended density wave interaction. For example the excitonic instability set up in the indirect semimetal $TiSe_2$, and running back someway towards TiS_2 [44], brings a state which, although taking on the overlap wavevector (π, π, π), displays an atomic displacement pattern involving not the LA mode, as in a standard charge density wave(CDW), but a TA mode [45, 46]. It should be noted here that in density waves of all types the shifts of the atoms from their pre-displaced locations frequently can be appreciably larger than is directly manifest from the lattice parameters themselves. With $2H-TaS_2$, Ta shifts of 0.1 Å bring only 0.01 Å changes to a_o, whilst in $1T-TaS_2$ with Ta shifts approaching $\frac{1}{2}$ Å even these for a long time escaped being registered. The 'Martensitic' changes developed within the $Z = 2$ A15 unit cell of V_3Si and Nb_3Sn similarly entail significant homopolar atomic pairings within the cell (below 16 K in the former, 48 K in the latter) which stand little betrayed by a_o itself. For the A15 materials these changes do not break crystalline symmetry, as a result of the direct nature of the band overlap there, but for the case of the pnictides and FeSe a slight, symmetry-breaking, periodic lattice distortion almost ubiquitously shows up at lowered temperatures, encouraged by the soft layered form of their crystal structures. One senses this orthorhombicity to emerge as countering outlier to the potential superconductive instability. In the familiar CDW responses of 2H- and $1T-TaS_2$, at first sight hexagonal and trigonal like their host structures, there in fact occurs comparable slight loss of symmetry to orthorhombicity and triclinicity respectively [46]. Such symmetry breaking often arises in response to small additional constraints, such as the requirement for favourable c-axis stacking—not just of the CDW itself but also the entrained PSD (periodic structural distortion) as well. In the current case there in addition is the question of magnetic coupling. We shall return to these sensitive matters in sections 8/ 9.

The scenario envisaged then for the present superconductivity is as follows. The RVB condition ties up a great many of the spins in resonant non-magnetic pairings, promoted by the basic $Z = 2$ unit cell with its strong four-fold n.n. Fe–Fe π/π^* interactions. This pre-pairing of the bulk of the spins ultimately overrides the partnering drive towards a spin density wave. What the direct spin pairing accomplishes is to predispose the developing excitonic instability towards superconductivity, and, provided the potential lattice instability can be held off (often via substitutional or non-stoichiometric change) it becomes favoured option under the advancing correlation. The superconductivity finally achieved develops, as with the HTSC cuprates, in the highly favourable circumstance of pre-paired bosonic entities positioned degenerately with the residue of fermions. Together the two populations become incorporated into one overall superconducting state to build a T_c much elevated in the highly resonant crossover conditions able to emerge under coordination unit shape ideality. Such a resonant boson–fermion crossover route to HTSC has a long history in the theoretical literature, e.g. Friedberg and Lee's papers of 1989 [47]. A considerably expanded exposition of this route to high T_c very recently has been released by Byczuk and Vollhardt [48].

In the case of cuprate HTSC, I have over the years in an extended series of papers developed a detailed scenario based on such boson–fermion degeneracy, grounded in the mixed-valent situation prevailing there [49]. However with cuprate HTSC the bosonic pair is conceived as emerging essentially *within* a Cu–O coordination unit as local shell closure p^6d^{10} entities, these generated as long-lived fluctuations within those coordination units being most driven towards trivalency by the highly localized substitutional and interstitial introduction of holes into the parent Mott insulators. I have introduced in order to describe such electron double-loading proximate to these sites the shorthand notation $^{10}Cu_{III}^{2-}$. The degeneracy of this bosonic object with the Fermi energy of the remaining free carriers comes by virtue of the very marked negative-U standing of that state, as the oxygen-p and copper-d states relocate strongly upon the termination of the $pd\sigma/\sigma^*$ interaction at shell closure. This electronic rearrangement and the ensuing induced superconductive outcome inevitably must within the narrow band system leave its mark in strong lattice changes, such as soft modes, unusual isotope effects, etc. However it remains in essence an electronically driven phenomenon. There is no retarded electron–boson mediated coupling here. The electron system itself is directly responsible. The above critical negative-U situation is closely related to that which initiates disproportionation in say $CsAuCl_3$ or $BaBiO_3$, where

$$2\,^9Au(II) \rightarrow \,^8Au(III) + \,^{10}Au(I),$$

and

$$2\,^1Bi(IV) \rightarrow \,^0Bi(V) + \,^2Bi(III).$$

These changes respectively involve d^{10} and 'lone-pair' s^2 shell completion. For the mixed-valent setting of the doped cuprates such double-loading is however not frozen in, but proceeds via the dynamic boson–fermion degenerate resonance to enable the realization of HTSC and extensive pair coupling. In the present case of the pnictides and FeSe the situation advocated is not quite so dramatic. The pre-formed pairs issue now not from double-loading essentially *on individual* coordination units, but from RVB-controlled spin pairing *between* coordination units. In the prevailing semimetallic environment, the bosonic pairs of the bonding VB are able to transfer across into the degenerately resonant Fermi sea. The success of the overall pairing, original and induced, in establishing a superconducting outcome of note depends upon the fact that the small semimetallic overlap is indirect and hence subject to the further correlation-driven effects of the excitonic insulator process. The potential for the above procedure accordingly is as statistically remarkable as that being claimed for the cuprates. It stands just as sensitive in its detailed outcome to modification by applied pressure, chemical doping, structural perfection and distortion.

The slight distortions so frequently developing in the pnictides manage very effectively to hamper the above scenario. Not only do they break symmetry, but they facilitate too an entrée to magnetism and spin-pair collapse as RVB coupling is disturbed. The rise and fall of T_c under hydrostatic

pressure, or chemical pressure, or substitutional and non-stoichiometric doping become then not so transparently related to the concomitant changes in coordination unit shape and bond splay angle α, and the key role that this latter plays. For example with LaOFeAs under hydrostatic pressure, T_c mounts not actually from a drawing closer to shape ideality but because it brings elimination of the orthorhombic distortion. One is required to bear clearly in mind too the distinction in effect that hydrostatic pressure has here upon the 1111-system as against chemical pressure, from say substituting La by the smaller Nd. The primary effect of *hydrostatic* pressure on a *simple* layer compound like FeSe is disproportionately to cause a reduction in height of the softer vdW region of the structure. As the sandwiches concertina into this region, the process brings a decrease in α. Of itself this should take FeSe to the *left* on figure 1, further away from shape ideality and toward lower T_c. Such a fall in T_c would be precisely the opposite of what the above chemical substitution within the 'intercalated' layers secures through Nd substitution into La-1111, the basally constricting effect now driving the material on figure 1 *toward* shape ideality (lower α) and to a higher T_c. That FeSe in fact experiences a *rise* in T_c under pressure is very likely the consequence of its significantly augmented 3D band dispersion better facilitating inter-sandwich pair transfer. FeSe is in this respect structurally unique on account of its empty vdW region. 'Intercalated' LiFeAs, for which α likewise lies below ideal, and with a Mössbauer spectrum providing no sign at low temperatures of ordered magnetism or structural distortion, indeed exhibits the expected decline in T_c under pressure [50].

At this point it will be a good test of the above general understanding to see if we can identify a dozen or so observations, hitherto often bringers of mystery and confusion to the literature, that now are able to receive ready clarification.

6. Shedding the mysteries

6.1. Indications of resonant behaviour in the vicinity of T_c

Several people have noticed that as one of these materials, whether under pressure or chemical stress, is taken closer to shape ideality and the optimization of T_c, the transition actually appears to get sharper. This is odd as the inevitable inhomogeneity in a high pressure cell usually leads to the reverse effect. It suggests the fine-tuning of a resonance effect. It is accompanied by expansion in the range and intensity of the linear-in-T resistivity found to show up universally in these materials directly above T_c [26b, 51]. Such a temperature dependence, which in the cuprates is very pronounced, has been taken in [49d] as evidence there of dominant boson–fermion scattering in the prevailing mixed, non-Fermi liquid condition. It is to be distinguished from that coming in the higher temperature incoherence regime.

A good monitor of whether or not standard Fermi liquid behaviour stands behind the superconductivity developed in FeSe and the pnictides is the thermodynamic measure afforded by ΔC_p, the jump in heat capacity across T_c. In BCS mean-field theory $\Delta C_p/\gamma_n T_c$ (where γ_n equals the normal state

electronic specific heat) takes the constant value 1.43. With the present materials it pointedly has been commented that the discontinuity appears more variable, and a very recent paper from Bud'ko *et al* [52] shows the way to systematizing this. They observe that over a wide range of materials in the 122 family the size of $\Delta C_p/T_c$ augments with T_c strictly as T_c^2. This constitutes a prime indicator once more of the resonant nature of the events being studied. If ΔC_p were to adjust linearly in step with T_c, while at the same time γ_n were actually to drop off linearly with the growth in T_c, then we would arrive at the above outcome. The number of effective fermions appears diminished as T_c climbs.

6.2. Further evidence of a narrow normal state fermion pseudogap forming around E_F

The sign of the Seebeck coefficient (controlled by $-\mathrm{d}\sigma/\mathrm{d}E$) being positive in FeSe over the low temperature range somewhat above T_c, in which $\rho \propto T$, signals for this l.t. range a dominant *valence* band carrier number and/or mobility [53a, 53b]. As in SmFeAsO$_{0.85}$, once above this range, S swings strongly negative to show by 110 K a *high* broad maximum, ~ -50 μV K^{-1} or more in Sm 1111-material [53c]. Such strong correlation effects also are on display in the significant temperature dependence of the Hall coefficient—see section 7. Additional direct evidence that due to strong correlations a form of deep pseudogap is present about E_F, over a considerable range above T_c, is provided by ultra-high resolution photoemission using a laser-excited spectrometer. It supports a steadily deepening DOS dip below ± 10 meV [54].

6.3. The shift in the Uemura plot

The striking thing about the Uemura plot (in addition to the fact that it gathers in all the exotic superconductors) is that its straight-line dependence of T_c upon n_s (the superfluid density) runs parallel to that for bosonic condensation. The plot finds itself displaced, however, significantly to the right (i.e. to larger n_s) as compared with the former. This finding would imply that to attain a desired T_c, n_s stands considerably higher than would be necessary were *every* pair of fermionic quasiparticles to constitute a fully effective boson. Viewed from the perspective of a given measured n_s value, T_c is down by a factor of about five on the associated T_B. From this it is clear the *crucial* boson population in place is much below n_s. Despite *all* the carriers ultimately becoming taken into the superconducting condensate, the majority are not those responsible for driving T_c to such heights. Such a circumstance was very evident in the data from YBa$_2$Cu$_3$O$_7$, where all the *chain* electrons are in the end taken into the condensate, but with virtually no change brought to T_c. The data which Uemura has to hand to generate these plots usually come from μSR precession signal relaxation rates measured in a magnetic field greater than H_{c1} (i.e. in the vortex state). The very large signal decay rate that was found in [55] for LaOFeP as compared with La(O$_{0.92}$F$_{0.08}$)FeAs marks how the quasiparticles in the phosphide are incapable of building a bosonic population of the same magnitude as that achieved with the arsenide. Note

F substitution in the latter material, by elimination of the orthorhombic distortion (and T_N), drives T_c up there despite interfering with the e/h balance. We earlier saw how the phosphide resides much farther from shape ideality. The impaired degree then of bosonic resonance produces not only a reduced fermion–boson interchange, but it encourages in addition the resurgence of magnetic fluctuations, changes which together result in a much lowered T_c.

6.4. A closer look at the pseudogap from NMR/NQR experimentation

Perhaps the clearest view of what is afoot here comes with the NMR results of Grafe *et al* [56], collected both for 'e-doped' La(O$_{0.9}$F$_{0.1}$)FeAs and pure LaOFeAs. (The 122 family [57] and FeSe [24c] insert certain complications better inspected separately, but all the data fall into the same general pattern.) The most striking feature is that the Knight shift, regardless of which atomic site type is being probed, senses a single spin fluid and one that, as with the bulk susceptibility, is remarkably low in magnitude (and away from stoichiometry free from any trace of ordered, local moment behaviour). Furthermore K_s is pointedly temperature dependent, settling to its minimum value only as $T \rightarrow 0$ K. Above T_c, K_s mounts steadily very close to linearly with T. All this speaks of a correlation-driven pseudogap, much as develops in the cuprates below $p = 0.185$. The pseudogap is non-states-conserving and distinctly unusual in that it does not lead to any weight-displaced peaks, just as much so for the Knight shift spectra as for the spin–lattice relaxation rate spectra. The absence of a Hebel–Slichter peak, along with the sharp fall off directly below T_c in $1/T_1T$ versus T plots as T^3 or steeper (again as with the cuprates) has led to talk of d-wave superconductivity and nodes in the superconducting gap. The latter complex and important matter again is best dealt with subsequently via other more direct techniques. For the moment it suffices to concentrate upon the relaxation data above T_c. Here once again regardless of which nuclei in the unit cells one actually selects to sense the spin–lattice relaxation, there occurs little evidence of standard local moment formation, of their ordering, or of spin-fluctuation scattering therefrom. Conversely the relaxation data do not follow the simple Korringa form ($1/T_1T$ = const.) of a classical metal either. Instead $1/T_1T$ picks up precisely the same variance as did the Knight shift [56] in being $\propto T$, i.e. $\propto \chi_{spin}(0, 0)$, i.e. $\propto$ the *fermionic* DOS—meaning the latter was being pseudogapped. That the various nuclei monitored each track the same temperature dependence means spin excitations have become suppressed uniformly over all q.

The sharp transfer shown above in $1/T_1T$ versus T at T_c, from variation above T_c as T to variation below T_c as T^3 or greater, is not so readily evident with BaFe$_2$As$_2$ and FeSe, especially the former. Prior to reaching T_c, over a range of 100 K in BaFe$_2$As$_2$ [57] and of 75 K in FeSe [24d, 58], one witnesses a significant growth in fluctuational scattering that appears not tied to any particular point in the Brillouin zone. The latter accordingly is *not* a reflection of the antiferromagnetic order present in these materials when at higher temperatures, in particular when undoped. Note

the *Knight shift* actually stays virtually unperturbed right across T_c, but the above additional scattering and spin–lattice relaxation in fact terminates abruptly somewhat prior to T_c. The latter evidently has nothing to do with impurities or two-phase behaviour. Tellingly it becomes more marked, rather than less so, as the pressure on the above materials is increased [24d, 59], tracking in this the rise there in T_c. The way I would suggest this low temperature scattering be understood is that it issues from the RVB/excitonic insulator/boson–fermion milieu itself. Under pressure, or in a more ionic setting such as that provided by BaFe$_2$As$_2$, the coupling of the lattice to the correlated, semimetallic system slows the fluctuational rate there to a level at which it becomes registered by the NMR probe, i.e. to $\omega < \sim 10^7$–10^8 s^{-1}. I see no justification to start turning here to standard antiferromagnetic spin fluctuations as responsible for the superconductivity, any more than I do with the cuprates, although the details of what is happening clearly are a matter to be pursued below.

6.5. Information from inelastic neutron data on the 'resonance peaks' and spin gaps

Because people endlessly look to parallels with the cuprate HTSC materials, it frequently has been presumed that the unsubstituted pnictides are simple antiferromagnets—as if complementary to LaCuO$_4$ or YBa$_2$Cu$_3$O$_6$. However the magnetic ordering, met with in LaOFeAs at 140 K [60], is not into a classic Néel state, and nor indeed is it into a classic spin density wave state either. On the one hand it shows spin wave excitations which are significantly gapped at low energy, and on the other it does not closely follow the Fermiology and take up an incommensurate **Q**-vector. Instead *inelastic* neutron scattering work reveals a strong, non-dispersing excitation at (π, π) for temperatures in the range 250–100 K, this scattering peaking quite sharply in intensity (over the above temperature range) at an energy transfer of around 8.5 meV. Note in all the pnictide families, the magnetic wavevector extracted from the *elastic* magnetic Bragg peaks is similarly set at (π, π, π), the corner of the primitive parent tetragonal zone—hence the source of the confusion.

As is to be seen from figure 9, in order to attain the observed magnetic cell would in a tight-binding picture rely on Fe–As–Fe superexchange, parallel in direction to the tetragonal cell edges and communicated via a pair of Fe–As (or Fe–Se) bonds subtending angle α [60]. The antiferromagnetic cell universally is observed in the company of a slight symmetry breakage to orthorhombic *Cmma* of about $\frac{1}{2}$%, much as might be thought to arise from magnetostriction under the basal orientation of the spins. The latter are all set parallel and antiparallel to b_O, the slightly longer basal axis for the *orthorhombic* cell [60]. As tetrahedral shape ideality is approached under pressure or via the action of substitutional doping, it would appear that the above magnetic exchange steadily becomes superseded on cooling by direct spin coupling between nearest-neighbour Fe sites. These, recall, lie two to each tetragonal cell in the 45° directions, and even in Ce-1111 ($a_o = 4.00$ Å) stand only 2.8 Å apart [61]. In
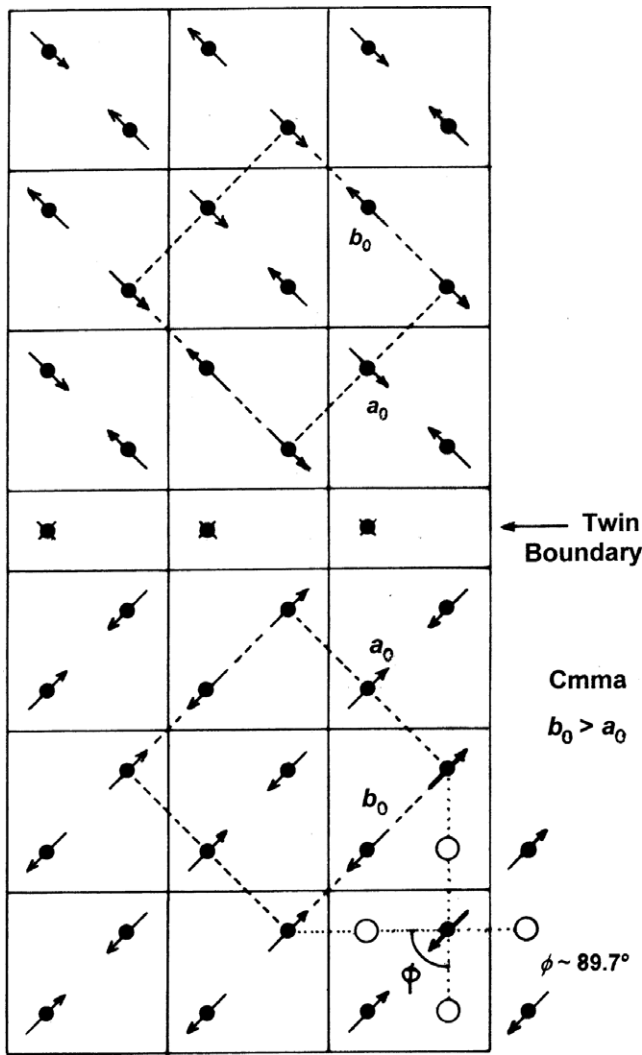
Figure 9. Illustration of the magnetic cell and the spin order assessed by neutron diffraction to hold for some way below T_d in many of these materials. The $\sqrt{2}$-by-$\sqrt{2}$ orthorhombic magnetic cell is indicated centred about a Fe site in a parent tetragonal cell (presented here in 'second setting' to emphasize the equivalence of its two Fe atoms). In the portrayed antiferromagnetic array such order would be in keeping in a local modelling with superexchange coupling interaction J_2 borne through the intervening As atoms stationed in the sheets above or below the Fe sheet as the case may be. In the low temperature condition the dominant interaction becomes direct intracellular spin pairing between the two Fe atoms there. Near T_c^{max} in the spin-gapped conditions so developed no magnetic LRO ultimately remains, and an RVB state is acquired in which all spin alignment orientations have become equivalent. The observed orthorhombicity recorded with almost all of these materials at low temperatures is thus necessarily not the consequence of magnetostriction—as indeed it was not above T_{SDW} (SDW: spin density wave) either. (Following convention the axes for the orthorhombic cell are labelled such that $b_O > a_O$.) Throughout as T goes down the static susceptibility declines linearly.

figure 9 the basic tetragonal cell, observe, has been positioned in 'second setting' (see section 3) to emphasize the equivalence of its two Fe atoms. RVB correlation-driven pair coupling would not necessarily demand any expansion here of the 'magnetic' cell, unlike the $\sqrt{2} \times \sqrt{2}$ expansion actually

being witnessed. Evidently things become considerably more intricate and interesting, as we shall find in section 8.

Note with either orientation of the antiferromagnetic orthorhombic cell included in figure 9, the two Fe atoms within each *individual* tetragonal cell are everywhere spin-opposed. This fact serves to emphasize the ease with which these materials are free to slip from the long-range order (LRO) site-moment organization of 'high' temperature antiferromagnetism over to SRO bond pairing or to RVB as correlation conditions become appropriate down towards T_c.

While for systems near shape ideality the spin susceptibility on cooling becomes basally isotropic and experiences a steady decline, such that in due course the systems become spin-gapped and effectively non-magnetic, this does not imply FeS, say, will have become *on-site* $S = 0$ like FeS_2. Rather we have a spin pseudogap condition resembling the one in the cuprate HTSC materials. As T in LaOFeAs drops below a potential low T_c this spin gapping extends up rapidly to higher energy to expose by 7 K a sharp 'resonance peak' at 12 meV [62]. In the case of 'e-doped' $Ba(Fe_{1.85}Co_{0.15})As_2$ the spin gap (as measured on compressed powder) is found fully opened initially only to 3 meV, but once well below T_c (26 K) the final resonance peak in evidence (formed again at the π, π equivalent) materializes up at 14 meV [63]. Taking the latter feature to identify $2\Delta(0)$ the energy converts here to the equivalent of $4.3kT_c$. With reference to the classical mean-field (s-wave) value for the ratio $2\Delta(0)/kT_c$ of 3.54 the above figure would mark a strong-coupling situation.

The reason why, within the present modelling, one can associate the above resonance peak energy with $2\Delta(0)$ is that it is perceived as being yielded by the RVB bosonic spin pairs, and in the global superconducting state these pairs have stabilized to lie below E_F by binding energy $\mathcal{U}$ per electron. To generate two independent fermions from such an $S = 0$ bosonic entity demands essentially an $S = 1$ spin flip, precisely as is secured in inelastic neutron spin-flip scattering. The difference between the present case and what is understood as occurring in the HTSC cuprates is that the boson in question now has been sourced from within a couple of coordination units, whereas in the cuprates it was effectively sourced by just the one such unit presenting p^6d^{10} shell-filling [49c]. In the cuprate case the extent of the mixing and coupling between the bosons and the degenerate fermions proves in consequence the greater and T_c the higher. The gap function $\Delta(T)$ measured in the HTSC cuprates emerges even less classical in form than what is seen here with the pnictides.

It will be good to have single crystal data from the various pnictides in due course to sharpen up these observations and to permit a more precise and meaningful comparison between the different systems over the matter of α-ideality. Qualitatively however the association of the resonance peak, strongly in evidence once below T_c, with the dominant pair binding energy looks well founded. A very recent paper from Zhao *et al* [64] dealing with $Ba(Fe_{1.9}Ni_{0.1})As_2$ ($T_c = 20$ K) has just reported that in a strong magnetic field the size of both T_c and the intensity and energy of the resonance indeed become simultaneously suppressed.

6.6. The bosonic mode as registered by optical infrared (IR) spectroscopy

Timusk and co-workers following their ground-breaking work upon the cuprates [65, 66] have now for a pnictide superconductor obtained a comparable extraction of the boson coupling function $\alpha^2 F(\omega)$ from the measured optical scattering rates, $1/\tau(\omega, T)$, following a maximum entropy deconvolution routine [67]. IR reflectance measurements were made on a single crystal of $(Ba_{0.55}K_{0.45})Fe_2As_2$ with $T_c = 26$ K, and expose changes to the spectrum arising below 300 K over the entire energy range under 150 meV. Below 100 K new features peak up strongly there into a doublet at 10 and 30 meV followed by a broader hump centred at 90 meV (720 cm^{-1}). Although the pseudogap forming in $1/\tau(\omega)$ falls in the phononic range, the measured temperature dependence and spectral details are not consistent with a phononic origin. Remember the system is a metal and phonons then figure only weakly in the spectrum. Boeri *et al* [39] have calculated the coupling parameter ascribable to phonons to be no more than $\lambda_{ph} = 0.21$, whereas the current experiments and analysis uncover λ values already ten times greater than this by 80 K, and growing to 3.42 by T_c. As was stated above, we are looking below T_c to a value of the energy for the bosonic resonance of about 15–20 meV. In practice to extract the actual boson energy from the self-energy related reflectance traces calls for detailed analysis, as has more recently been carried through with the HTSC cuprates in [66]. With the latter materials the boson energy itself emerges as being roughly 40% smaller than the energy of the associated reflectance feature, and accordingly now the strongest spectral feature, standing at just under 30 meV, would fit current expectations. In bosonically induced global superconductivity note that T_c and $2\Delta(0)$ always are going to reflect the weakest link in the overall move to condensation.

The uppermost anomalous feature around 90 meV, being sited toward the lower end of the range where $\rho \propto \omega$ holds, looks in contrast to be connected with the changes bestowing incoherent behaviour; changes that for the cuprates were claimed to incorporate strong lattice relaxation [49d].

6.7. Injections from ARPES

The ARPES results are forthcoming mainly from the Ba-122 family because of the availability of suitable crystals. They fall into several strands and appear sufficiently in line with expectation to generalize. As with the cuprates they support the above discussion in manifesting the presence of a kink in the low energy dispersion curves [68], indicating thereby the action of the intersecting bosonic state in imparting strong renormalization to the effective masses of the carriers around E_F. The reduced overall width of the V.B being reported expresses likewise the appreciable correlation beyond that carried by the LDA exchange approximation. The semimetallic pockets as disclosed by ARPES, although somewhat smaller in size than those calculated, do, however, remain in the anticipated locations in the B.Z. A more striking observation is that once below T_c the superconducting gaps on those pockets are shown not to be equal in size—although seemingly roughly

isotropic in direction. In this they are reminiscent of what was found with MgB$_2$ (semimetallic between B–B p$_{x,y}\sigma$ and p$_z\pi$ bonding and antibonding states, and exhibiting a T_c of 40 K) [69]. Again now the largest of the gaps arises in a hole band and is located about Γ.

Drawn from the more recent literature, reference [70] undertakes for Ba-122, pure and substituted, a detailed ARPES study above T_c of the LDA band shifts and the mass renormalizations required to agree with the X point data ($\equiv \pi, \pi$ in the basic tetragonal zone), taken from its two electron pockets. The results display surprisingly little sensitivity as to whether the sample in fact is h-doped (K$_{0.4}$) or e-doped (Co$_{0.06}$). Such ARPES data are in line with the more detailed numerical assessments acquired from the dHVA/dHS experiments. (The latter are pursued, recall, within the 'normal' state at very low temperatures after suppression of the full superconducting condition by the application of magnetic fields in excess of H_{c2}, or rather H_{irr}, i.e. >30 T [29].) As stated back in section 4, the overall effect of the electron correlation active near E_F is to deepen the pseudogapping there via a shifting of both sets of bounding bands by ~ 50 meV, the h-bands around Γ being moved downwards, the e-bands around π, π moved upwards.

As regards the situation *below* T_c and direct observation of the superconducting gap sizes, recent ARPES work from [71] comes for a $K_{0.4}$ sample ($T_c = 37$ K) to the following estimates $\Delta_\alpha^\Gamma = 8.5$ meV, $\Delta_\beta^\Gamma = 4.0$ meV, and $\Delta_{\gamma,\delta}^X = 7.8$ meV. These values drop in their less-substituted sample ($K_{0.25}$, with $T_c = 26$ K) by about 30%. Such a reduction in gap size with fall in T_c (appropriately found too to scale with H_{c2}) is very different from the form of pseudogap behaviour witnessed in the underdoped cuprates. Although a pseudogap is forthcoming in the pnictides it is not associated with the 'dichotomy' in gap sizes witnessed with the cuprates. There, what is more, the behaviour around the Fermi surface was highly anisotropic under an order parameter of d$_{x^2-y^2}$ form. Now in the pnictides this most certainly is not the case. The latter matter has been probed directly in the scanning SQUID microscopy work of Hicks *et al* on F-substituted polycrystalline Nd-1111 [72], and no π phase shifts are in evidence, no orbital currents being observed. Such a finding does not mean the order parameter here is of simple s-wave form. As with MgB$_2$ the order parameter actually would appear to be extended s-wave ($s^\pm$: $\Delta(\mathbf{k}) = \Delta(\cos k_x + \cos k_y)/2$), this entailing a sign change in Δ between the hole pockets at Γ and the electron pockets at π, π. Such an order parameter actually introduces no nodal behaviour into the current semimetallic Fermi surface. Good reason exists theoretically to anticipate the above outcome [73]. However again we shall find below how things turn out somewhat more complicated in practice.

6.8. Revealing input from electronic specific heat work

It is possible the two-peak behaviour extracted from electronic specific heat data for FeSe [33] is making record of the above two-gap state, much as previously has been recorded in the cases of MgB$_2$ [74] and NbSe$_2$ [75], and similar attention should now be paid to LiFeAs ($T_c = 20$ K). For the latter

present indications are that the jump in $\Delta C_p^{el}/\gamma_n T_c$ across T_c is considerably below the BCS value of 1.43 [76]. By contrast Mu *et al* [77] working with $(Ba_{0.6}K_{0.4})Fe_2As_2$, where T_c = 36.5 K, emerge with a $\Delta C_p^{el}/\gamma_n T_c$ value there of 1.55. This now is somewhat greater than the mean-field value, and it arrives in conjunction with a very sizeable value extracted for γ_n of 63.3 mJ mol^{-1} K^{-2}. The latter proves an order of magnitude greater than was obtained with F-doped LaOFeAs [78]. The likewise high value of the ΔC_p^{el} jump at T_c in the 122-material means that the feature stands out clearly there in the raw data. The empirical value of $\Delta C_p^{el}/T_c$ is up very close now to 100 mJ mol^{-1} K^{-1}. Such magnitudes both for γ_n and $\Delta C_p^{el}/T_c$ (remember we are dealing with a semimetal) speak of strong correlation and coupling. For a simple metal $\gamma_n = \frac{2}{3}\pi^2 k_B^2 N(E_F) \cdot (1 + \lambda)$. In the present case one may accordingly attribute the above results to elevated values for both $N(E_F)$ and λ over those expected under electron–phonon coupling, arriving from the action associated with the pseudogap, including raised values for m^*, and they match our electronically based understanding of what drives the pnictide superconductivity. The level of differentiation observed between one pnictide material and another in these matters comes, as previously was indicated, from the degree of proximity to shape ideality. Thus the $\Delta C_p^{el}/T_c$ jump observed in LaOFeP-based material [79] stands well below that seen even with LaOFeAs.

Recently Bud'ko *et al* [52] have arrived at the very telling observation, when examining a whole series of $BaFe_2As_2$-sourced materials, that $\Delta C_p^{el}/T_c \propto T_c^2$, this relation involving such a large coefficient of proportionality that virtually two decades in $\Delta C_p^{el}/T_c$ are spanned here. Because with standard superconductors $\Delta C_p^{el}/\gamma_n T_c$ = a constant, behaviour like this would intimate linear augmentations as T_c both to $N(E_F)$ and λ, as shape ideality and the resonant superconducting condition are approached.

Given the extent and level of the analysis which Mu *et al* [77] have undertaken on their $C_p^{el}(T, H)$ data, it is rather surprising they did not attempt a multigap treatment in light of the clear manifestation of a secondary hump within their $C_p(T)$ trace around 20 K, much as is exhibited by MgB_2 and $NbSe_2$. Already we have observed from the ARPES work that the order parameter for pnictide systems when approaching shape ideality is not simple s-wave, but multigap $s^\pm$, wherein different levels of gapping are supported across the semimetallic k-divide. Accordingly the gap value of 6 meV extracted by Mu *et al* and subsequently inserted into their analysis must stand as average value over the span of 'local' values, such as those cited in section 6.7 deriving from the ARPES data. Ma *et al* do however very elegantly and effectively probe the magnetic field dependence of the specific heat data to confirm that their $BaFe_2As_2$-derived material displays node-free superconductive behaviour. This result once more is in striking contrast with their earlier results on F-substituted LaOFeAs material, for which the analogous data would clearly indicate the occurrence in that case of nodes in the superconducting gap [78]. This has not simply to be taken as marking a distinction in behaviour between the 122 and 1111 families: F-substituted SmOFeAs is known to show

node-*free* behaviour [79]. It is that matter of shape ideality again (see figure 1).

6.9. Comparable results from optical measures of the electronic kinetic energy

It is very striking that the Drude IR edge in the high T_c pnictides stands clearly displaced towards low frequency as compared with what LDA band structures would lead one to anticipate. Qazilbash *et al* [80] very recently have made a close assessment of this correlation-driven shift as a function of temperature both for LaOFeP and LaOFeAs. By conversion of the measured optical conductivity, $\sigma_1(\omega)$, through to the associated optical scattering rate, $1/\tau(\omega)$, it immediately becomes apparent that, as with the HTSC cuprates [81], the correlations run at such a level as to drive the carriers in these semimetals close to incoherence. $h/\tau(\omega)$ falls only just short of kT, and in fact climbs linearly with T, pursuant to the linear rise with T in evidence in the dc resistivity just above T_c [51]. Such behaviour is very like that recently re-examined by Cooper *et al* [82] for the HTSC cuprates, and which I interpret as resulting from boson–fermion scattering in the resonant negative-U crossover circumstance prevailing there [49e]. In the cuprates the high degree of correlation in evidence reflects their proximity to the Mott transition. Now in the pnictides however it is sourced by proximity to shape ideality and the associated deep semimetallic pseudogapping. The resonant bosons are this time of RVB origin and experiencing excitonic insulator coupling to the fermions. Because LaOFeAs stands much closer to shape ideality than does LaOFeP, such correlations, and hence T_c, are greater in the *former*. This marks a striking inversion of fortunes as compared with Mott-driven correlations, where a phosphide always will exhibit stronger correlations than does the corresponding arsenide, due to the more advanced p–d mixing in the latter—witness CrP versus CrAs, NiP versus NiAs (see [2a, figure 1]). Qazilbash *et al* [80] numerically assess the situation via appraisal of the optical conductivity through the integral— $h_{C_o}/e^2 \cdot \int_0^{\omega_c} 2h/\pi \cdot \sigma_1(\omega) \cdot d\omega$, this being equivalent to the electronic kinetic energy $K_{exp}(\omega_c)$. An appropriate frequency cut-off of 3000 cm^{-1} has been applied here. The authors make comparison then of this K_{exp} with direct evaluation of the quantity K_{th} drawn from the much more lightly correlated LDA band structure. The experimental value for K proves diminished relative to the latter by a factor of 2–4 times—and the arsenide indeed stands here the *more* correlated of the two. In [80] this was presented as a mystery.

6.10. The penetration depth results

In like vein to the above, we in Bristol initially were perplexed by the conflicting outcome to our penetration depth measurements, made first on Sm(O/F)FeAs [83] and then subsequently on La(O/F)FeP [30]. In line with the above it gradually became clear why the former system yielded the exponential variation of a fully gapped response for $\lambda(T)$, whilst the second system exhibited a low temperature power law variation for $\lambda(T)$, in keeping with a partially gapped status. The node-free behaviour of the $s^\pm$ order parameter is

secured with the shape-ideal, spin-paired, small overlap Sm system, whilst a node-bearing response, materializing under order parameter $\Delta = \cos k_x/2 \cos k_y/2$, is adopted with the system well removed from shape ideality, in which magnetic input is not being fully subsumed into RVB and the deep spin-singlet pseudogapping to follow. Both FeSe [84] and also BaFe$_2$As$_2$ and derivative material [85], which, when unsubstituted, stand at some distance from shape ideality and RVB behaviour, do not display a truly exponential variance in $\lambda(T)$, but show at low T a T^2 dependence, as for dirty s-wave. The 'dirt' now however is intrinsic, with the hole and electron pockets behaving differently.

Although the two above order parameters each are covered by representation A$_{1g}$ within point group D$_{4h}$, their geometrical arrangement of nodes is so different that it is hard to see how the situation encountered can slide continuously from the one to the other without some first-order break being encountered, especially when folding in the changing role of the lattice. We shall return in section 8 to examine the light recent experiment casts on this matter—once more a situation clearly more complex than was originally suspected. Prior to looking into this, some further comments are first in order on the role of chemical substitution.

## 7. A further look at chemical substitution

The 'doping' terminology so widely used with the pnictides is, as with the cuprates, one that does not serve the field well. It is one that with the cuprates I sought from the start to avoid, advocating use of the terms 'substituted' and 'interstitial' [49a, 49b]. The reference point for an HTSC cuprate is to the d^9 Mott-insulating parent and the half-filled d$_{x^2-y^2}$ band. By the time metallicity is met with, however, the number of active carriers is rapidly departing from the number of monovalent 'dopant' centres introduced. In (La$_{2-x}$Sr$_x$)CuO$_4$, etc 'p' in reality monitors the Cu(III) count, not the carrier count. Now, too, Co substitution in say Ba(Fe/Co)$_2$As$_2$ does not simply see electrons added to the conduction band, but also fills in holes in the valence band of the parent compound—this time no Mott insulator but a band semimetal. The false parallel being imposed on the pnictides has come from a desire to endow the present antiferromagnetic parents with comparable characteristics to the Mott-insulating cuprate parents like La$_2$CuO$_4$, and then to drop into attributing the superconductivity to spin fluctuations. It is an attribution made too lightly, and one which patently is as false now as then.

In both fields T_c climbs as low energy spin gapping grows. With the pnictides the latter is fostered by the move to shape ideality within the tetrahedral coordination unit, with a favouring of local moment-free RVB spin pairing, as opposed to antiferromagnetism—even if more related to SDW-type nesting, without the Hund's rule type behaviour seen in hexagonal FeS. In the cuprates there comparably is in play a shape-dependent aspect to the rise of T_c, expressed there in the degree of distortion away from ideality of the octahedral Cu–O coordination unit in the form of a strong

Jahn–Teller type c-axis elongation. This distortion is greatest in the Hg-cuprates for which T_c comes to its maximum. With the cuprates the primary effect is to diminish the basal lattice parameters and thereby hold down magnetic moment formation, extending the spin gap to its maximum energy— and specifically beyond the $S = 1$ spin-flip excitation energy of the sustained superconductive pairs. The precise aim in selecting the ideal substituent with the cuprates is to secure the lowered basal lattice parameter and full suppression of free moments precisely as the key concentration of Cu(III) centres of $p = 0.16$ is reached. The latter is a percolation/charge-stripe dictated level [49, 86]. With the pnictides it is evident from experiment that likewise there exists a comparable drive to offset maximal T_c from the simple stoichiometry of the parent. This action now though is not to generate metallicity or to acquire some specific level of charge deviation, but rather to perturb the system sufficiently that the excitonic coupling across the semimetallic divide then favours superconductivity as alternative to the vying instabilities of SDW and CDW/PLD (periodic structural distortion). Here disordering is clearly more quickly advanced by substituting directly on the Fe site [87] than it is when disturbing the electron/hole balance at one remove, as in substituting Ba with K [88]. Breaking the regularity of the site up-spin/down-spin d-electron array automatically will favour RVB over well-structured antiferromagnetic order. The current $Z = 2$ cell geometry helps greatly in this regard, as too does the dominantly 2D-coupling of the layer compound environment.

It is highly informative to consider precisely what Co substitution into BaFe$_2$As$_2$ [87] is bringing about. Just 8% Fe replacement leads to a complete elimination of the parent SDW ($T_{\text{onset}} = 135$ K), the maximal T_c of 23 K then immediately being acquired. This substitution in fact is associated with a reduction in average lattice parameter [89], as if resulting from low-spin d^6 Co(III). The surplus electrons then must be delocalized over the Fe sites. That such disturbance promotes low temperature spin pseudogapping is registered both in ^{75}As and ^{59}Co NMR work [90]. No local moments are induced here, and the Knight shift data reveals a strong reduction in spin susceptibility with increase in x_{Co}—as with decrease in T and right from room temperature. By $x_{\text{Co}} = 0.1$, K_s has levelled out at a low and temperature-independent value, with the same being witnessed for $1/T_1T$. Both spin susceptibility and spin-fluctuation-induced relaxation rate have become invariant and small in the pre-superconductive range (as earlier seen in section 6.4 with the 1111-materials).

The present research from Ning *et al* [90] proceeds further and discloses, from study of the NMR lineshapes, that the changes are apparently associated with micro-inhomogeneity at the nanometre level, here the substitutive changes very locally controlling the detailed response. Such disturbance led within low-p cuprates to the development of striped behaviour, both fluctuating and frozen, but in the pnictides there as yet is no sign of comparable micro-organization. There are, however, indications of some macrostructural adjustment as the magnetic organization is disrupted and RVB takes over, as we shall see below. Ning *et al* in their very interesting contour plots of the NMR data, drawn up across the T–x_{Co}
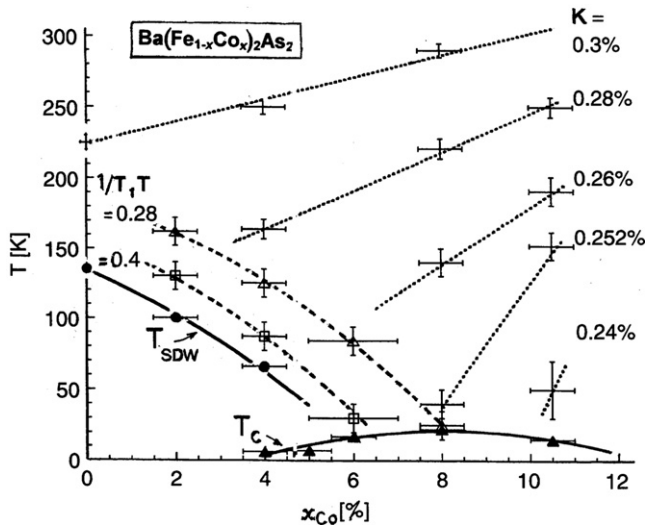
Figure 10. A view of the state of play in the T versus x_{Co} field for the system $Ba(Fe_{1-x}Co_x)_2As_2$ secured by Ning *et al* from ^{75}As NMR work [90]. The two heavy lines mark the onset temperatures of the SDW and of the superconductivity. The former state is lost as the latter is approached. At low cobalt content the superconductivity looks as if it would reach a $T_c \sim 40$ K were it not for the intervention of the SDW state with its spin-flip pair-breaking capacity. The dashed and dotted lines shown are contours in the T–x_{Co} plane of equal relaxation rate $1/T_1T$ and of equal Knight shift K. The spin–lattice relaxation rate is noted to rise sharply as the SDW condition is approached. Over the rest of the plane the Knight shift data reveal a steady growth in spin pseudogapping as T drops. A limiting minimum value for K_{spin} is reached as $K \rightarrow K_{chem} = 0.225$. Remember the spin component is directly proportional to the quasiparticle spin susceptibility. When presuming Δ_{pg} to be T independent, it is possible to extract a pseudogap value ≈ 500 K or 40 meV over the range where T_c maximizes. (Reproduced with permission of *J. Phys. Soc. Japan*: copyright 2009.)

plane, reveal $1/T_1T$ and K_s to have dropped respectively to 0.28 and to 0.25% by the point at which T_c globally maximizes (23 K, here at $x_{Co} = 0.08$). Their plot has been reproduced with some amplification as figure 10. Many, pursuing the spin-fluctuation scenario for the superconductivity, would like to point to such a figure as indication of magnetic, quantum critical behaviour, with the latter somehow associated with seeding-out superconductivity. My own reading of the above figure is that in pure $BaFe_2As_2$ superconductivity would have arisen near 40 K were it not for the preferred adoption of the SDW state onsetting at 138 K. The two states are seen as competitors—not working in tandem. The spin pseudogap energies as deduced from this NMR work amount to around 500 K or 40 meV.

One might ask on what experimental grounds such a viewpoint, such an extrapolation as the above, is based. I would like to point here to the high pressure results secured by Kotegawa *et al* [91] from unsubstituted $SrFe_2As_2$. The latter enters a SDW state below 200 K for which the onset temperature is found to decrease rather little as a function of pressure. Then suddenly between 3 and $3\frac{1}{2}$ GPa it rapidly declines directly to be replaced by superconductivity with a T_c of 34 K. $T_c(P)$ above this pressure would again look to extrapolate back to ~ 40 K at $P = 0$. Given the inhomogeneity

within the pressure cell, this data strongly suggest a first-order replacement of the one ground state by the other. What has swung the balance now in favour of superconductivity? It is known that pressure deepens the spin pseudogap, just as did Co substitution and the lattice parameter decrease which it introduced. A further comparable and striking result is obtained when working in the *isovalently* 'anion'-substituted system $BaFe_2(As_{1-x}P_x)_2$ [92]. Despite this replacement of the arsenic by phosphorus actually forcing the system further away from shape ideality, the disorder that it introduces and the reduction in basal parameter are sufficient for a while to favour superconductivity as ground state across the substantial range from $P_{0.30}$ to $P_{0.65}$. From there once again $T_c(x_P)$ would extrapolate back under the SDW state of pure $BaFe_2As_2$ to a value of 40 K. In a small range around $x_P = 0.3$ the two states appear to coexist (probably micro-inhomogeneously—see below). $BaFe_2As_2$, note, does itself in fact become superconducting under 4 GPa, but by then with a T_c of only 29 K [8].

Being layer compounds the pnictide materials can rather easily be perturbed in the third dimension, and that probably is how K substitution of Ba in 122-material ought in large measure to be regarded. However the charge change simultaneously introduced makes such attribution there rather tenuous. A very striking new result has, however, just been secured pointing in that direction. Intercalation of $SrFe_2As_2$ by water vapour has been discovered to bring about superconductivity with T_c at 25 K [93]. There is no charge change here, just perturbation of the structure and of the Fe-based 3D spin ordering. A rather similar result was experienced with trigonal prismatically coordinated TaS_2, where intercalation by a wide variety of organic molecules suppresses the CDW there in favour of superconductivity.

Above in section 2 we have noted that in LaOFeP the LaO there plays the role of a monovalent lanthanyl ion. The La atom itself here is on the outside of the LaO sandwich and feeds its third electron over directly into the P atom. The latter atom hence forms an integral part of the La atom's coordination shell. In a great many La compounds its coordination shell is expanded beyond six; for example it is eight in the d^1 layer metal LaI_2 [94]. What further pseudo-ions might now be intercalated to play the same role here of supplying electrons to the FeP sandwiches, and be able to prise the latter even further apart? The answer, steadily building, is a great many. A particularly striking one is Sr_2ScO_3, or rather a block twice that thickness, the FeP layers now becoming spaced by in excess of 15 Å. This Sc(III) phosphide product is *non*-magnetic and is superconducting with a T_c of 17 K [95]. In marked contrast the corresponding arsenide is this time non-superconducting, in fact non-metallic, and it exhibits Curie–Weiss behaviour at the Fe sites [96]. Such inversion here between arsenide and phosphide looks to be due to the lifting of the semimetallic overlap—see [96a, figures 3 and 4] and [96b, figure 4] for the effect on ρ, χ, S and R_H. Then with $(Sr_2\underline{V}O_3)_2 \cdot Fe_2As_2$ and reduction again to the a_o parameter (and α), a remarkable re-emergence of T_c at 37 K is witnessed [97]. Note here that, as with LaO, both above inserts inject into the Fe–X sandwich one electron per intercalate molecule, procuring thereby our

basic 'stoichiometric' d^6 Fe(II) electron count. Analogous results are now forthcoming by insertion of various complex titanates [98]. Whether or not all these intercalates in fact stand commensurate with the host is yet to be determined. Incommensurateness would add further to the disordering process. 'Misfit intercalation' is well known for layer systems, $(BiS)_{1.11} \cdot NbS_2$ being a prime example [99].

The complete break-through above in $(Sr_2ScO_3)_2 \cdot Fe_2As_2$ of a semiconducting gap at d^6 arrives within a material that remains tetragonal at low T. There is even greater danger of this occurring whenever $e - h$ nesting drives the system into a low temperature density wave state, cutting down further the residual Fermi surface. Several weakly substituted, high e/h balance, systems have actually been witnessed, through study of their Hall coefficients, to suffer 'metal/insulator' conversion below T_{DW}, in particular when they stand close to high shape ideality and already contain a well-developed DOS pseudogap; Sm, Ce and even $La(O_{1-x}F_x) \cdot FeAs$ [6a, 100, 101] are cases in point, as well as $BaFe_2As_2$ [102]. A close study of the Hall coefficient in the Sm-1111 system, made both in the high- and low-field regimes and as a function of fluorine substitution, has demonstrated how at low x the number of free carriers declines exponentially once below T_{DW} [103]. No carriers of course means no superconductivity. Sm-1111 with $x = 0.12$ sees n become $<10^{19}$ cm^{-3} by 4 K. A final elimination of the DW state at $x = 0.18$ frees the potential in the system to manifest superconductivity immediately with $T_c^{max} = 54$ K. The fact that in $(Sr_2VO_3)_2 \cdot Fe_2As_2$ T_c climbs yet further from 37 to 46 K under pressure [104] would similarly indicate that a certain DOS level and metallicity is best suited to uphold the excitonic superconducting state.

8. The engagement of the lattice

Above we have seen some of the effects wrought by chemical substitution upon the lattice and T_c, and at several stages have noted earlier the sensitive response of T_c to pressure. A further striking observation related to the lattice, very recently reported in [105] is the change to T_c in strained (unrelaxed) epitaxial thin films generated by altering the lattice mismatch to the substrate. Using substrates of $YAlO_3$, $LaAlO_3$, $(La, Sr)(Al, Ta)O_3$ and $SrTiO_3$ (of increasingly larger a_o) it has for the case of $Ba(Fe_{0.9}Co_{0.1})_2As_2$ been found possible to induce a linear rise of several degrees in T_c through altering the c/a ratio conferred upon the film. From the lattice parameter details supplied it is apparent that α rises and T_c falls with YAO as substrate, whilst with LSAT and STO α falls and T_c rises. LAO affords virtually a perfect lattice match for the Co-substituted 122-material (where α is somewhat above ideal) and T_c remains unchanged. Such effects inevitably imply there are going to be isotope effects in these systems—and there are [106]—but that does not mean T_c is primarily controlled by electron–phonon coupling. In any reasonably narrow band circumstance it becomes impossible to decouple charge or indeed magnetic effects from the lattice.

At T_{SDW} the measured thermal expansion coefficients $\alpha(T)$ show something like a 20% drop [107], a change that in fact follows in quick succession, for the 1111-LnO

family, upon a comparable decrease at a sharply defined structural distortion temperature occurring some 5–25 K above T_{SDW} [107]. I would like to read this overlying structural transition as a CDW. Certainly it is not a consequence of magnetostriction because it clearly precedes the magnetic order (and indeed outlives it). However, at the same time, it presents the same essentially $\sqrt{2} \times \sqrt{2}$ increase in basal cell geometry (see figure 9). In this for 1111, as with all related families, the increase involves transferring from the 4 Å-edged primitive tetragonal cell to a face-centred cell of orthorhombic form for which $a \approx b \sim 5.6$ Å. In all cases the level of symmetry breakage is slight $\{o = (b - a)/\frac{1}{2}(b + a) \sim 0.5\%\}$, although the transition itself can manifest a small first-order component [108, figure 3]. With unsubstituted 122-material, the magnetic and the distorted conditions are (untypically) entered into simultaneously, and this has the profound effect of changing the spin-fluctuational behaviour monitored by neutron scattering from being 3D-Ising-like to being 2D-Ising-like [109]. The intimate effect of the slight structural change upon the magnetism is echoed by an equally striking effect of the lattice distortion in regard to the subsequent superconductivity, as evidenced in the isotope effect. Whether with $(Ba/K)Fe_2As_2$ or $Sm(O/F)FeAs$ different phonons have been observed to experience different isotope shifts, but in each individual case both T_c and T_D are found remarkably to show identical shift exponents [106a].

However, as we have witnessed above, where T_c is highest, as in Sm-1111 or in FeSe under P, the Mössbauer data makes very evident that the ordered antiferromagnetism and much of the paramagnetism have by then been shed. It is clear, what is more, neither magnetic order nor the orthorhombic lattice distortion (LD) are obligatory forerunners to the emergence of pnictide superconductivity, each being absent in LiFeAs [6a] and $Sr_2ScO_3 \cdot FeP$. In the case of FeSe the (initial) orthorhombically induced quadrupole splitting of the Mössbauer 'singlet', moreover, becomes lost under pressure *as T_c rises* [26b, figure 2(b)]. Such sensitive interplay and competition between these three aspects, SDW, CDW/PLD, and superconductivity, would suggest all emerge from the same origin. All three are able to stand as expressions of the excitonic insulator interaction, and extremely small free energy changes are implicated in tipping the balance between the possible ground states. These ground states may involve a coexistence of SDW and/or CDW/PLD with the superconductivity, or the superconductivity can exist alone. In fact where T_c is highest the latter circumstance would look to hold. Where these 'manifestations' coexist, this either may be accomplished homogeneously (as witnessed previously in $2H-NbSe_2$, with the presence below 6 K of both CDW/PLD and superconductivity), or it may involve heterogeneous phase separation into micro-regions, the latter variously dominated by one or another aspect. A rather similar situation was encountered in the HTSC cuprates in the case of $La_2CuO_{4+\delta}$ under certain interstitial oxygen overloads, δ. There, as was revealed by use of dark-field electron microscopy, some regions are antiferromagnetic, and others superconducting, dependent upon the local organization of the interstitial content [110].

In the present $\sqrt{2} \times \sqrt{2}$ structural transitions little or no discontinuity in underlying basic cell volume is discerned, but there is a sharp change, as pointed out above, in thermal expansivity, the latter becoming somewhat reduced below the transition (see [108], figure 3]). Where perhaps more revelatory effects are detected is (as with MgB_2) to specific phonons. As previously has been indicated, some exhibit an isotope effect whilst others do not [106a]. LeTacon *et al* [111] working with small $Sm(O/F) \cdot FeAs$ crystals and employing inelastic x-ray scattering very recently have reported *oppositely signed*, doping-induced, renormalizations for phonons having energies lying close to either side of a potential resonance at 23 meV. It is too early as yet to come to firm conclusions here, since LeTacon *et al*'s results are for 300 K only. It will be most interesting to pursue what developments arise through T_{CDW}/T_{SDW}. Anyone who doubts the marked response of the lattice to what is occurring electronically out well in advance of T_{CDW}/T_{SDW} should look at the recent resonant ultrasound spectroscopy results from Fernandes *et al* [112] revealing very strong softening of the shear modulus.

Figure 11(a) represents the type of CDW/PLD $\sqrt{2} \times \sqrt{2}$ supercell array compatible with the presence of RVB coupling and able initially to uphold tetragonal symmetry within the present unusual network of edge-sharing tetrahedra. The original primitive tetragonal Fe–X units are marked out in 'second setting' and the $\sqrt{2} \times \sqrt{2}$, 45°-rotated, (tetragonal) supercell shown dashed. At the latter's centre lies a resonating square plaquette of four spins. If these units were to relax somewhat, one ought to be able to pick up appropriate superspotting by electron microscopy if not by x-ray and neutron diffraction. Unfortunately in many of these materials this will not be easy. To date there is definite indication of additional diffuse scattering being present above the orthorhombic symmetry-breaking distortion temperature, and we shall look at this matter in more detail in section 9. Whether under instigation from non-stoichiometric e/h balance, or from substitutional disorder, or from c-axis stacking adjustment, figure 11(b) illustrates how the above tetragonal array of bonds is able readily to give place to orthorhombic distortion of the $\sqrt{2} \times \sqrt{2}$ supercell simply by this freezing out of 1D pair-striped domains, these latter taking up twinned orientation as portrayed in figure 11(b). Alternatively, given the propensity of the systems for face-centring, one might well encounter the 1D arrangement of dimer pair bonding portrayed in figure 11(c), again in conjunction with its twin.

9. Microstructural behaviour in FeSe and the pnictides, and what it is able to reveal

The microstructure of twin formation arises from local relief of lattice strain as the new state breaks lattice symmetry. The faster the temperature decrease and the larger the impurity/structural defect density to initiate twin boundary pinning, the smaller will be the typical twin domain size. This fracturing of the crystalline continuity is to be distinguished carefully from inhomogeneous two-phase behaviour, both as to its origins and form. The latter process follows breakdown
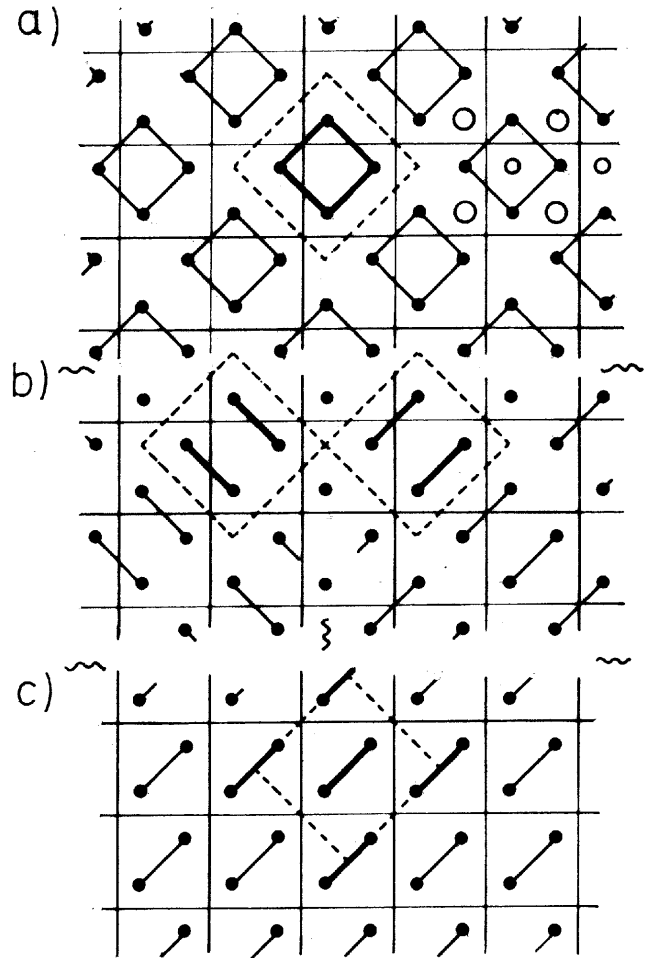
Figure 11. Charge-, spin- and lattice-coupled RVB arrays. At the top an $S \to 0$ quadrimer array is portrayed that does not break tetragonal symmetry. In the centre are two relaxed, orthorhombic dimer twin settings. The bottom section gives an alternative orthorhombic arrangement of pair bonds taking the same basic $\sqrt{2} \times \sqrt{2}$ cell size.

in solid solution formation between components A and B over some concentration span. In the thermodynamics controlling solid solution, free energy lowering is in general enabled through the downward bowing of the configurational entropy term, but this form can be disrupted by the local A–B interaction becoming repulsive over a certain concentration range (or by the descent of new ordered states). Such repulsion can result from a simple size effect mismatch between components or more interestingly be electronically based, as when trying to mix a Mott insulator with a band material. If the above changes become sufficiently pronounced as to produce an actual upward dimple in the free energy curve then the system finds it energetically advantageous to break up into a two-phase mix, with individual compositions and their relative amounts set by the 'common tangent' construction. The latter equates $\partial G/\partial n$ at the two tangential points, defining thereby state equilibrium (see [113] for the physics behind the construction of phase diagrams). Sometimes component A will tolerate little or no solid solution with B. Then on the phase diagram, A defines virtually a 'line phase', flanked to either side across two-component spans

by inhomogeneous two-phase behaviour. Iron monoselenide would appear to find itself in such a circumstance in relation to potential non-stoichiometries $Fe_{1-\delta}Se$ and $FeSe_{1-\varepsilon}$. Fe_7Se_8 is a well-established phase along the former path. The unfortunate thing about our target composition, FeSe, is that this itself actually falls within a two-phase range of composition. A line phase (or virtually so) does in fact separate the two non-stoichiometric and indeed two-phase ranges linked above with 'iron selenide', but the stable homogeneous single-phase material emerges as being slightly selenium-poor at $FeSe_{0.974}$ [108, figure 5] (or equivalently, so far as the mass ratio goes, iron-rich at $Fe_{1.02}Se$ [53a, figure 3(b)]). Stable non-stoichiometric 'defect compounds' of this type are not uncommon among transition metal materials, the superconductor 'TiO' being an extreme case in point. Even GaAs is, note, very slightly off-stoichiometry as crystallized from its melt. Phase separation is not confined just to the iron selenide superconductor [53a, 108], but appears now widespread amongst the pnictide systems too [114; (Ba/K)Fe_2As_2], [115; Sm(O/F)FeAs]. Between pure and substituted conditions clearly quite strongly repulsive interactions must arise to introduce 'dimpling' so ubiquitously into the free energy curves. Such materials problems can be a real menace when trying to deal with an already complex and delicate situation, but maybe with regard to the electronic problem now in hand one can turn this complexity of form to some advantage.

There arises comparably intricate and widespread action in regard to the orthorhombic distortion and its precursor thermal behaviour. Again the thermodynamics can suggest processes and provide illumination as to what is going on. We cited earlier the case of the thermal expansivity data from Klingeler *et al* [107] for members of the 1111 family. The effect of the $T \rightarrow O$ transition (at T_D) upon $\alpha(T)$ was to cause a positively signed anomaly, whilst, conversely, the effect of the SDW onset (at T_M) upon $\alpha(T)$ is to generate a negative anomaly. Application of the Ehrenfest thermodynamic relation necessitates then that dT_M/dP will see reduction in T_M, whereas pressure increase will bring a rise to T_D, thereby increasing differentiation between the two transition temperatures. Any potential *tetragonal* CDW will have lost out here in stability range to the 1D orthorhombic state, while the ordered magnetic state likewise will have become more confined in phase space.

In looking at the detailed outworking of these matters let us first begin with FeSe, before delving into the extensive substitutional changes of the 1111 and 122 families.

In FeSe the Fe–Fe distance is only 2.66 Å, as against 2.80 Å in $BaFe_2As_2$ and 2.85 Å in LaOFeAs. At 90 K there takes place in 'FeSe' a loss of structural symmetry much as occurs in $BaFe_2As_2$ at 138 K and at 150 K in LaOFeAs; namely a slight distortion of the original tetragonal structure into an orthorhombic, $\sqrt{2} \times \sqrt{2}$ supercell, wherein b/a duly comes to differ from unity by just $\sim\frac{1}{2}$%, angle ϕ (see figure 9) departing from 90° by only around 0.3°. Recall from what was said though in section 5, despite such small modifications to the cell itself, the atomic shifts internal to the unit cell need not be insignificant. Indeed in $Fe_{1.01}Se$ a splitting in Fe–Fe

separations of 0.012 Å is acquired by 20 K [116], while in LaOFeAs the difference is marginally greater at 0.014 Å [117]. The really striking distinction between the two materials, however, is that with FeSe no magnetic transition follows, unlike with stoichiometric LaOFeAs, etc for which elastic neutron scattering work finds a magnetic moment $\sim0.3\mu_B$ ordered in the spin arrangement of figure 9. No such SDW development is experienced with near-stoichiometric $Fe_{1.01}Se$, the Mössbauer trace reported in [116] as elsewhere being throughout of a magnetic singlet state. The dominant RVB-type spin pairing implicit here in the selenide has to be a reflection of its much closer Fe–Fe spacing. LiFeAs, for which Fe–Fe is 2.68 Å very much as with FeSe, indeed displays no SDW in advance of T_c (=20 K) [6, 118], and, what is more, seemingly no orthorhombic distortion either, though that now needs closer examination by TEM. (Note in LiFeAs α is only 102.9° [6b].)

Since $Fe_{1.01}Se$ presents its orthorhombic distortion without any SDW the distortion clearly cannot be magnetostrictive in origin. A CDW automatically is indicated. Let us examine more closely then the detailed form of the PLD suggested in [116] from their combination of low temperature synchrotron x-ray diffraction and transmission electron microscopy. The latter experiments reveal that the distortion in fact is of lower symmetry than the customarily quoted Cmma form (space group #67, D_{2h}^{21}). The latter group simply would express the $\sqrt{2}$ expansion from the parent tetragonal cell (space group #129, $P4/nmm$) plus the newly acquired cellular orthorhombicity. However the diffraction results and in particular the TEM data make it here apparent, through the occurrence of 110-type superspotting, that the correct space group has to have shed the horizontal glide plane 'a' (the former 'n'-plane of the tetragonal parent). The observed absence of 100-type super-spots would, however, signal the retention of C-face-centring. That there no longer exists the half-integer horizontal glide, linking neighbouring Fe atoms in the x_O direction in the basal plane supports the fact that those atoms have become slightly dimerized as intimated in the previous paragraph. The situation expressed by the data is as conveyed above in figure 11(c). The space group looks to have contracted here to #35, $Cmm2$ C_{2v}^{11}, although the actual loss of symmetry could in reality be somewhat more severe as the selenium atoms accommodate to maintain Fe–Se bond lengths. Note the arrangement of figure 11(c) betokens a bond-centred CDW as against some site-centred restructuring of the charge distribution. It is a prime expression of RVB coupling having tied up the residual spin into now static, non-magnetic, $S = 0$ dimer entities—a scaled-back version of what is encountered in d^5 arsenopyrite FeAsSe (see section 2). Of course for our material in due course to exhibit superconductivity necessitates that such 'pre-formed' pairs are or can be rendered electronically mobile, and that a semiconducting gap of the severity developed in FeAsSe, Ti_2O_3, etc is avoided.

The above may well provide the key to understanding the additional striking discovery made in [116]. $Fe_{1.03}Se$, placed at the opposite edge of the 'line phase' to $Fe_{1.01}Se$, proves remarkably different from the latter in its properties. Not

only does it not become orthorhombic at low temperatures but, furthermore, not superconducting either [116]. However what McQueen *et al* do observe from their TEM work on $Fe_{1.03}Se$ is that its structure clearly is not covered by tetragonal space group $P4/nmm$, any more than it is either by orthorhombic groups $Cmma$ or $Cmm2$. It would appear from the simultaneous presence of both 100- and 110-type superlattice spotting that a strictly $\sqrt{2} \times \sqrt{2}$ enlarged tetragonal cell has been taken up. Direct lattice imaging of the sample reveals intensity fringing with a basal spacing of 5.4 Å, or twice what is witnessed with $Fe_{1.01}Se$. It is just feasible that what is being registered here for the current d^6 electron-count system is an array of spin quadrimers, as introduced in section 8 and portrayed in figure 11(a). Strong, high-order, structural groupings are a feature of many transition metal compounds under the appropriate electron count; e.g. the quadrilaterals in d^3 ReS_2 [1] and the triangles in d^2 $LiVO_2$ [119], with weaker such groupings, as noted earlier, occurring in hexagonal FeS [12] and NiAs [120]. The TEM diffraction plate included by McQueen *et al* [116, figure 3(d)] shows, from the appearance of both 100-type and 110-type spotting, that the basal glide and C-face-centring elements have each been abandoned in the prevailing space group, although the latter clearly retains overall tetragonality. Group $\bar{4}2m$, #111 D_{2d}^1 would accommodate these changes, the Fe atoms being located here in its four-fold degenerate, type m sites. Perhaps this quadrimer condition is now too correlated, too non-metallic, for the semimetal to uphold superconductivity (at least above the 0.5 K checked to). Certainly the resistivity is significantly higher here than even with $Fe_{1.01}Se$ [53a, figure 5].

Interestingly a comparable distinction in diffraction and resistivity behaviour has been picked up by Wang *et al* [121] using thin films of 'FeSe' grown epitaxially on MgO (provided the films are unrelaxed, possessing thicknesses below 150 nm). When grown with the substrate held at $500\,^\circ C$ the product is just as for bulk $Fe_{1.01}Se$, but if the substrate is held at only $320\,^\circ C$ the behaviour of the film becomes much more like $Fe_{1.03}Se$, with no low temperature orthorhombicity and no superconductivity. Strikingly a growth habit difference occurs between the two products. The $320\,^\circ C$ product, from the a_o fringing present in its TEM lattice image, involves a somewhat strained (expanded), non-face-centred, tetragonal [001] growth mode, whereas the $500\,^\circ C$ product shows [101] growth with fringes perpendicular to [$1\bar{1}1$]. As stated, the latter product exhibits both orthorhombic distortion and superconductivity at low temperature; the former does neither. It is crucial now to discover how TEM imaging and diffraction from specimens like these alters upon cooling below room temperature.

A similar data gap exists for the temperature evolution of the Fe site Mössbauer signal forthcoming from the two types of product. Precisely how does the quadrupole splitting in these materials alter with T? Figure 6 in [53a] from McQueen *et al* would suggest a distinction between the two in the quadrupole-split line-broadening observed at 5 K as compared with 295 K, it being greater in $Fe_{1.03}Se$ than in $Fe_{1.01}Se$. The Seebeck data in the same paper [53a, inset to figure 5] seem to signal the possibility of an event at 130 K in the case of $Fe_{1.03}Se$. There the magnitude of S becomes largest, at $-16\ \mu V\ K^{-1}$,

this following (for both compositions) a sign change from $+$ to $-$ below 230 K. The results in [53c, figure 4] are very similar. Is there any further indication in the literature of some 130 K event in less closely characterized 'FeSe'? Figure 7 in [122] would suggest the occurrence of a slight alteration there to the change in c/a with T, whilst figure 3(a) in [123] claims to see a sharp discontinuity at this temperature in paramagnetic magnetization.

At this point the reader perhaps feels the distinction between $Fe_{1.01}Se$ and $Fe_{1.03}Se$ is impenetrable—or worse—not worth penetrating, a detail ascribable to 'dirt'. However one very powerful microprobe of any complex situation is always NMR. In [24d] from Imai *et al* we already have observed how in FeSe the Knight shift signal from $S = \frac{1}{2}$ ^{77}Se suffers a strong reduction in magnitude with temperature, beginning right from the phase stability limit of 500 K. This reduction in K_s (or equivalently χ_{spin}) is virtually identical for both $Fe_{1.01}Se$ and $Fe_{1.03}Se$ [24d, figure 3]. There is a marked difference between the two, however, when it comes to measuring the *integrated* intensity of the NMR line. With $Fe_{1.03}Se$ the latter is invariant below 100 K (although the line broadens somewhat), but with $Fe_{1.01}Se$ a clear drop off in *intensity* is recorded coming *in advance* of T_c. This distinction becomes much more marked under applied pressures of up to 2.2 GPa (for which T_c does not exceed 15 K)—and it occurs without change to K_s itself. How can 50% of the NMR signal have disappeared in $Fe_{1.01}Se$ under these conditions, yet not in $Fe_{1.03}Se$?

That this 'wipeout' is fluctuational in nature immediately is made evident upon turning to the relaxation rate data. $Fe_{1.01}Se$ below $\sim$130 K deviates from its hitherto linear-in-T fall in relaxation rate $1/T_1$, and $1/T_1T$ actually turns up sharply below 90 K (T_D) to produce a marked hump. The latter hump (when integrated) becomes more pronounced under pressure and always occurs at a T in advance of the growing $T_c(P)$ [24d, figure 4]. The fluctuations have widely been viewed as due to spin fluctuations. As these fluctuations take on RVB form and freeze out as dimer pairs the susceptibility experiences 'wipe out'; the system becomes spin pre-paired and ready to move forward to the special superconductivity of these materials [24d, figure 3]. $Fe_{1.03}Se$ lacks all aspects of this fluctuation freezing. With $Fe_{1.01}Se$ under pressure as the freeze-out arrives at higher T so too $T_c(P)$ moves up. Note this spin freezing is not spin ordering because that would bring a splitting of the Knight shift spectrum, which is not seen.

A related technique to examine the local magnetic condition on short timescales is μSR. Being an expression of precisely where the muon localizes prior to decay, the technique enables one to assess the homogeneity of the sample via observation of the spin depolarization rates for the muons as they precess, either in a small applied magnetic field, or in a self-generated field. Below T_c and for fields greater than H_{c1} the sample is penetrated by flux vortices wherein the field, being non-uniform, leads to non-synchronization of the individual site precessions, and hence decay of the overall precession signal. This depolarization rate is directly related to the penetration depth, and hence to the local superfluid density n_s. In a significantly phase-separated situation one is in a position then to pick up multiple signal decay rates.

Such phase separation quickly was registered by following μSR decay in a field transverse to the spontaneous field direction when using a sample of slightly 'underdoped' (Ba/K)Fe$_2$As$_2$ (T_c = 37 K) [114a]. There it was deduced that only 25% of the sample actually was superconducting, with 50% locked into the SDW condition, proportions that change with T. To confirm such a phase separation, zero-field scanning magnetic force microscopy was undertaken (at 26 K), and the granularity of the condition became directly evident. By Fourier analysing the scanned image it was found that the typical span of the magnetic segments was about 650 Å, which is not too dissimilar from λ (and much greater than the stripe domaining of the cuprates). Both powder and single crystal neutron diffraction revealed this *electronic* phase separation to be occurring in material which crystallographically appears homogeneous and orthorhombic. There is comparable evidence the filamentary superconductivity recorded in Na$_{1-x}$FeAs occurs under very similar conditions [124].

Besides examination of two-phase structuring, μSR also allows equally valuable information to be extracted from the present materials below T_c in relation to the progressive development of the superconductivity across the semimetallic divide. Under pressure it proves possible specifically to track the developments of the penetration depths and the superconducting gaps as functions of $T_c(P)$. Using the theory introduced by Kogan *et al* [125] for a two-gap superconductor, Khasanov *et al* have been able to resolve the strikingly different behaviours exhibited in the Γ pocket and the zone corner pocket. Compressed powder samples of nominal iron selenide compositions FeSe$_{0.94}$ and FeSe$_{0.98}$ were measured and analysed by Khasanov *et al* [126] in this two-pocket manner. Over the pressure range up to 0.85 GPa, T_c rises smoothly from 8.5 to 13 K. Here $T_c(P) \propto \lambda^{-2}(0, P)$, as foreseen by Schoenberg. When decomposed into its two components, the smaller (X point) gap hardly alters in its Δ or λ (i.e. n_s) contributions to the sum, but for the larger (Γ point) gap these quantities each augment linearly as $T_c(P)$. The two components behave almost independently, the contribution of the smaller gap arriving only well below T_c, but the two sets of carriers still are sufficiently coupled that just the one overall T_c applies [126, figure 2]. This is a situation very like the relationship that the plane and chain carriers possess in YBa$_2$Cu$_3$O$_7$, where the additional superconductivity of the chains boosts λ^{-2} and n_s, but brings virtually no boost to T_c for the entire ensemble. Analogous behaviour recently has been reported for optimally substituted Sm(O/F)·FeAs by Weyeneth *et al* [127] employing a combination of torque magnetometry, SQUID magnetometry and μSR. As the applied field is increased to $\sim$1 T (a field way below H_{c2} for the material *in toto*) it is observed that the larger gap, as expected, is virtually field-independent, but the smaller gap is strongly suppressed. These experiments demonstrate conclusively that in these materials the high T_c behaviour is emanating from the RVB pairings of the zone centre pocket.

The above, in respect to FeSe, related to P being less than 0.8 GPa. Above this pressure a whole series of further new and highly illuminating phenomena arise. It for some time has been known that $T_c(P)$ shows a hiatus in its growth, with an actual minimum showing up in $T_c(P)$ between 1 and 2 GPa [128], prior to renewed rise to attain a T_c which peaks at over 35 K in the best samples under a pressure $\sim$10 GPa [26b]. The latter high pressure range is free from any pair-breaking scattering due to magnetic order, as is apparent from the Mössbauer spectrum there [26b, figure 2(b)]. The latter is of singlet form. Beyond 6 GPa there is, though, clear evidence of two-phase behaviour, with the development of a component that appears non-metallic. What, however, of the pressure range between 1 and 2 GPa, within which the T_c minimum occurs, and for which no Mössbauer results are available?

Upon returning to the μSR results of [126] for this range one discovers that it is a region in which a very large fraction of the overall sample opts to develop magnetic order. This order evidently coexists intimately with the superconductivity because the magnetic order parameter (onsetting between 20 and 40 K) drops away appreciably in amplitude as the superconductivity arrives near 12 K [126, figure 3]. Why should pressure have this interim effect of introducing magnetism to FeSe in this way? The answer has to lie in the fact that FeSe is a true layer compound, where c_o initially drops disproportionately rapidly with P, falling from 5.5 to 5.1 Å over the above pressure range [26b, figure 1(d)]. This decrease promotes the 3D magnetic coupling strength greatly. Ultimately the slower reduction in a_o and the ensuing increase in the direct basal Fe–Fe interaction tips the balance back in favour of RVB, and the superconducting T_c can rise again. It should be recalled here that FeSe has the smallest a_o of all these materials, even prior to the application of pressure, and now by 10 GPa it has declined a further 4%. Where such interaction between the competing superconducting and magnetic order parameters has similarly been directly recorded is in the small coexistence range existing in Ba(Fe$_{1-x}$Co$_x$)$_2$As$_2$ near $x = 0.05$. The latter observation was made by neutron diffraction, measuring specifically the effect on the magnetic order parameter. As Fernandes, Pratt *et al* [129] demonstrate in a full analysis of their data, it is observations such as this which confirm the superconducting order parameter to be here s^{+-} and not s^{++}.

10. Superconductivity of note in other homopolar bonded, semimetallic materials

The features which turn FeSe, etc into remarkable superconductors might then be listed as follows

 (i) homopolar bonding that brings considerable movement of the associated bonding and antibonding bands;

 (ii) a moderately complex crystal structure for which the symmetry is not too high and there result quite a number of bands;

(iii) a low-dimensional structure, here layered (but perhaps a chain or even an individual cluster structure would suffice), that affords ready intersite spin dimerization;

(iv) a moderately ionic system where strong local characteristics are still preserved and the carriers are not too delocalized;

(v) one, however, in which magnetism does not dominate;

(vi) a semimetallic situation to which structural dimerization has not brought the complete removal of free carriers;

(vii) a semimetal in which the overlap is indirect, bringing into play the instabilities of the excitonic insulator and boson–fermion degenerate tunnelling;

(viii) a semimetallic overlap that is not too great, limiting the level of screening of local action and also restricting Fermi surface nesting.

How has FeSe acquired such characteristics?

- Feature (1) comes from a structure in which the tetrahedral Fe coordination units share edges, bringing quite a short Fe–Fe nearest-neighbour separation.

- Feature (2) comes as the adopted structure is a non-symmorphic, tetragonal one in which $Z = 2$ (unlike its zincblende polymorph).

- Feature (3) represents a rather unusual circumstance for a monochalcogenide of a transition metal element, of being marginally stable here over the nickel arsenide structure, this seemingly on account of the current d^6 electron count and what this engenders near E_F.

- Feature (4). FeSe and even FeAs might still be classified to some degree as retaining ionic characteristics, evident from comparison with GaSe or AlAs.

- Feature (5). The NiAs-structured, $S = 2$ polymorph of FeS is strongly magnetic and metallic, characteristics avoided in our current system.

- Feature (6). Feature (5) came with the semimetallic, tetrahedrally bonded product. With the number of delocalized carriers rather low, the drive to dimerization is not then overwhelming.

- Feature (7) is the product of the basal glide plane in the adopted structure. The bosonic carriers degenerate with the C.B. fermions lie at the top of the M–M bonded V.B. at the Γ point, and are of low crystal momentum. The valence bands in question show virtually no dispersion along ΓZ, and at coordination unit shape ideality become locally spin-isotropic. It is for the bosonic pairs from these zone centre bands that superconductive gapping is high.

- Feature (8). If the semimetallic overlap becomes too large as in FeTe, or too small or even absent as in FeS, then the superconductivity becomes less striking or vanishes altogether.

Quite a lot of materials share of course many of the above attributes, and some indeed are superconductors that have caught attention in the past. As noted earlier, the A15's like V_3Si and Nb_3Ge are semimetals which display Martensitic dimerization, but this arises in a 3D cubic setting and the semimetallic overlap at Γ is direct [130]: T_c is limited to 23 K. The Chevrel phase superconductors like $PbMo_6S_8$ looked promising too. The Mo_6 M–M bonded octahedral cluster that supports E_F is however built into a 3D (cubic) structure, and the units are quite widely spaced. The A_3C_{60} Bucky Ball superconductors are in a not dissimilar situation, with alkali atoms intercalated between the C_{60} clusters to produce an open band situation. As was expressed in [131], I believe that the right way to address superconductivity in A_3C_{60} is of *pair*

tunnelling between the cluster balls. The C_{60} units, composed of weakly distinguished double and single bonds, encourage negative-U pre-pair formation, and the alkali ions set up a significant local perturbation on the structure and electronic environment. I expressed it a big mistake at the time to proceed with a rather standard MacMillan and Dynes type treatment as pursued by Schluter *et al* [132] and others.

Graphite is a semimetallic polymorph of carbon with a very limited carrier population. The band overlap here is direct, between p_z–p_z π-bonding and–antibonding states, and superconductivity when derived from this base by intercalation is only of low T_c. Where things have become much more exciting has been with MgB_2, a pseudographite intercalated by Mg^{2+} ions. Here both σ- and π-bonding states are involved in a situation in which the semimetallic gap now is indirect. A T_c of 40 K still has not deterred people from proceeding with a standard treatment in MgB_2, despite it being clear specific phonons contribute to coupling constant λ in a very anharmonic fashion [133]. It would seem MgB_2 is coming very close to kinship with FeSe. In fact all the above materials actually find accommodation on or close to the Uemura plot, wherein high T_c is acquired for remarkably small n_s values, as determined from penetration depth/μSR studies. Where the iron pnictide materials would seem to surpass MgB_2 in performance is that the homopolar bonded states in play at E_F are transition metal states and involve, beyond the primary σ-interaction, secondary π-interaction within the iron atom sublattice. This permits now a more variable density of states and somewhat greater flexibility of action, provided, that is, one can avoid the pair-breaking action of ordered magnetism. It could be thought one way to achieve the latter would be to turn to 4d and 5d materials, but this could lead to dimerization becoming too strong (witness NbO_2 versus VO_2), or to spin–orbit splitting introducing unwanted instabilities. It is notable, however, that the current iron pnictides will tolerate a considerable replacement of Fe by Ru without T_c falling too strongly, despite the broadening of the bands [134].

In truth the window of opportunity afforded by SmO·FeAs, etc is a very narrow one, and although we now see a plethora of new 'high T_c' superconductors, as opened up in [95–99] with $(Fe_2As_2)·(Sr_4(Mg, Ti)_2O_6)$, etc, these all prove variants on a very restricted theme. As was seen from figure 1 regarding the 1111 family, the response here to slight change is supersensitive and fascinating to follow. However the situation would appear not to offer great hope for emulating the remarkable heights reached in the equally sensitive cuprates with the resonance on show in $HgBa_2Ca_2Cu_3O_{16+\delta}$, and T_c under pressure of 165 K.

In closing three more contact points should be made. Firstly the excitonic insulator condition alone does not suffice to yield high T_c on the evidence of what is observed in layered $TiSe_2$ [135, 136] or pyrite β-SiP_2 [137]. Secondly β-ZrNCl (which is quite differently layered from the α-form), containing a strongly Zr–Zr bonded Zr bi-layer and supporting superconductivity around 25 K when intercalated with Li [138, 139], witnesses its superconductivity to maximize just prior to Mott localization [140]. (The α-form is a simple salt.) Notably this 4d-series superconductor again falls on the Uemura plot [55].

Finally we have the question of where we are proceeding with the remarkable superconductivity manifest in many elements under high pressure. For some time now we have been made aware of raised T_c superconductivity in group-B elements like silicon (12 K) [141], phosphorus, or sulfur in their high pressure polymorphs. Under pressure these elements move away from their low pressure often molecularized non-metallic structures to acquire low-dimensional network structures, bi-layered in the case of black phosphorus ($T_c =$ 14 K). With sulfur T_c reaches a value of 17 K [142]. All these superconducting forms are semimetals, and of course are homopolar bonded, retaining still a small nearest-neighbour count rather than shifting to simple 'close-packing'. ('Close-packing' is, note, 12 n.n atoms standing off at considerable uniform separation.) The inverse of the above process we now find happening in group I, II and III metals. These elements transfer under pressure into reduced coordination number structures—the sort of change existing between Al and Ga. The resulting structures can become very complex, sometimes incommensurate, or of the 'guest and host' type, a bit like boron [143]. Typically the phases where superconducting are semimetallic in form. We witness Li acquire a T_c of 20 K [144], and Ca and Y reach a T_c up around 25 K—and still rising under pressure [145]. Once more it appears we are seeing aspects here of what we have been discussing earlier in regard to the iron pnictides.

The message definitely in all this is to examine more low-dimensional, homopolar bonded semimetals—say perhaps CaSi$_2$ or a gallium or titanium boride cluster system.

11. Summary

The pnictide superconductors are indirect gap semimetals, appreciably more delocalized than the cuprates. Their unusual form of layered, tetragonal crystal structure is responsible for the semimetallic outcome. The latter is secured largely in consequence of the strong direct Fe–Fe bonding/antibonding interaction experienced here. This direct interaction leads to materials wherein the magnetic spin becomes locked, not in ordered magnetism, as with nickel-arsenide-structured FeS or FeP, but in RVB fashion. On cooling, the paramagnetic susceptibility becomes quenched linearly with falling temperature, and when/if ordered magnetism becomes realized at reduced temperatures it takes a low effective moment. Such ordered magnetism (plus its spin excitations, so damaging to superconductivity) can be suppressed by adding carriers to the materials, or often by applying pressure, increasing quasiparticle delocalization.

Being indirect gap semimetals, the materials are susceptible to excitonic insulator type electronic instabilities adopting the wavevector separating the electron and hole pockets. The magnetic order actually to emerge takes up this specific wavevector. Whenever such magnetic order appears, it always is prefigured by a slight structural symmetry breakage to orthorhombicity, this likewise displaying the above instability wavevector. Neither magnetic order nor orthorhombic distortion prove necessary forerunners to the superconductivity, LiFeAs being a case in point. All that is required is for a suppressed magnetic susceptibility, imposed by the dominant RVB coupling.

The dynamic bonding spin pairings of the carrier states around Γ are seen as constituting bosons, these resonant with the decoupled fermions in the quasiparticle pocket at the zone corner. The ensuing boson–fermion transfer is viewed as being responsible for the elevated T_c superconductivity of these systems. The superconductive gapping acquired is significantly different on the Γ and X point pockets, it being considerably greater on the former, from where the population of bosonic pairings originates and the action is governed.

The particular materials able to sustain the highest T_cs are those for which the paramagnetic susceptibility is small and the site moment most constrained, and for which the coordination geometry is moving toward being perfectly tetrahedral. The latter shape ideality has the effect of procuring degeneracy between the d$_{xy}$, d$_{yz}$ and d$_{xz}$ Fe–Fe pairing states, strengthening RVB, advancing correlation, opening a pseudogap, and promoting the excitonic insulator instability in a manner such as to favour superconductivity over an SDW or CDW end product.

The above three are competitor ground states. They can occur in conjunction, but then impair each other's order parameters, competing for the same electrons over a Fermi surface very limited in extent. T_c currently is greatest in fluorine-substituted SmO·FeAs, a system where shape ideality is close to being achieved, but which has to accept a considerable e/h imbalance in order to inhibit magnetic ordering. If it were possible to accomplish the latter via intercalation by a non-donor such as H$_2$O it might be possible to see T_c rise somewhat.

Superconductivity is not as spectacular with the pnictides as with the cuprates because the bosons generated by RVB coupling are not so robust as the carrier pairings created under the negative-U double-loadings within the mixed-valent environment of the HTSC cuprates. The pnictides, nevertheless, hold a good many features in common with the cuprates which can make the systems appear more similar than they truly are. In each case the strong electron–boson scattering renders the conductivity near-incoherent at raised temperature. The presence of a well-defined bosonic state leads to comparable IR optical spectra, and their spin excitation under spin-flip inelastic neutron scattering once more leads to a characteristic 'resonance peak'. Additionally there is the very similar NMR spin–lattice relaxation behaviour, particularly below T_c, while, of course, both families cluster about the Uemura plot, as revealed in μSR penetration depth studies.

With both families, since the controlling interaction is electronic, T_c is easy to manipulate by substitution or intercalation, and either set of materials readily descends into complicated microstructural behaviour, although in the pnictides there is nothing quite like stripe phase formation. For the cuprates such structuring has a strong Coulombic input, but the pnictides are more covalent and better screened dielectrically, despite their low carrier count. In the end the more ionic character for the cuprates stands as what upholds their remarkable, unique, negative-U state behaviour, and from this their truly high T_c superconductivity.

Acknowledgments

The paper is dedicated on the occasion of his ninetieth birthday to Dr Abe Yoffe of the Cavendish Laboratory, Cambridge—my former Research Supervisor and long term Editor to the forerunner of this Magazine.

References

[1] Wilson J A 1969 *Adv. Phys.* **18** 193–335
[2a] Wilson J A 1972 *Adv. Phys.* **21** 143–98
[2b] Wilson J A 1973 Around the Mott transition in binary transition metal compounds *Conf. Proc. 'Phase Transitions and Their Applications (May 1973, Penn State Univ.)* ed L E Cross (Oxford: Pergamon) pp 101–16
[3] Wilson J A 1984 *NATO ASI* B **113** 657–708
[4] Wilson J A 1985 *Mott Festschrift—'The Metallic and Non-Metallic States of Matter'* ed P P Edwards and C N R Rao (London: Taylor and Francis) chapter 9, pp 215–60
[5] Ishida K, Nakai Y and Hosono H 2009 *J. Phys. Soc. Japan* **78** 062001
[6a] Jeglič P *et al* 2009 arXiv:0912.0692
[6b] Pitcher M J, Parker D R, Adamson P, Herkelrath S J C, Boothroyd A T and Clarke S J 2008 *Chem. Commun.* 5918 (arXiv:0807.2228)
[7] Johrendt D and Pöttgen R 2009 *Physica* C at press
Johrendt D and Pöttgen R 2009 arXiv:0902.1085
[8a] Alireza P L, Ko Y C T, Gillett J, Petrone C M, Cole J M, Lonzarich G L and Sebastian S E 2008 *J. Phys.: Condens. Matter* **21** 012208
[8b] Colombier E, Bud'ko S L, Ni N and Canfield P C 2009 *Phys. Rev.* B **79** 224518
[8c] Kotegawa H, Kawazoe T, Sugawara H, Murata K and Tou H 2009 *J. Phys. Soc. Japan* **78** 083702
[9] Braithwaite D, Salce B, Lapertot G, Boudarot F, Martin C, Aoki D and Hanfland M 2009 *J. Phys.: Condens. Matter* **21** 232202
Mizuguchi Y, Tomioka F, Tsuda S, Yamaguchi T and Takano Y 2009 *Appl. Phys. Lett.* **94** 012503
[10] Bertaut E F, Burlet P and Chappert J 1965 *Solid State Commun.* **3** 335
[11] Takahashi T 1973 *Solid State Commun.* **13** 1335
Horwood J L, Townsend M G and Webster A H 1976 *J. Solid State Chem.* **17** 35
Gosselin J R, Townsend M G, Tremblay R J and Webster A H 1976 *J. Solid State Chem.* **17** 43
Leclerc A and Townsend M G 1978 *J. Phys. Chem. Solids* **39** 687
[12] Putris A 1974 *Science* **186** 431
[13] de Medicis R 1970 *Science* **170** 1191
[14] Figgis B N 1966 *Introduction to Ligand Field Theory* (New York: Wiley Interscience)
[15] Rueff J-P, Kao C-C, Struzhkin V V, Badro J, Shu J, Hemley R J and Mao H K 1999 *Phys. Rev. Lett.* **82** 3284
[16] Bullett D W 1982 *J. Phys. C: Solid State Phys.* **15** 6163
[17] Wilson J A and Pitt D 1972 *Phil. Mag.* **23** 1297
[18] Scaglotti M, Jouanne M, Balkanski M, Ouvrard G and Benedek G 1987 *Phys. Rev.* B **35** 7097
[19] Tsuji T, Howe A T and Greenwood N N 1976 *J. Solid State Chem.* **17** 157
Kjekshus A, Nicholson D G and Mukerjee A D 1972 *Acta Chem. Scand.* **26** 1105
Vaughan D J and Ridout M S 1971 *J. Inorg. Nucl. Chem.* **33** 741
[20] Vaughan D J and Craig J R 1978 *Mineral Chemistry of Metal Sulphides* (Cambridge: Cambridge University Press)

[21] Burgardt P and Seehra M S 1977 *Solid State Commun.* **22** 153
[22] Tandon S P and Gupta J P 1969 *Solid State Commun.* **7** 1793
[23] Nakamura T, Shimura T, Itoh M and Takeda Y 1993 *Solid State Chem.* **103** 523
For recent discussion of such matters see Sentel M, Kuneš J, Werner P and Kampf A P 2009 *Phys. Rev.* B **80** 155116
Eder R 2009 arXiv:0911:4236
[24a] McQueen T M, Williams A J, Stephens P W, Tao J, Zhu Y, Ksenofontov V, Casper F, Felser C and Cava R J 2009 *Phys. Rev. Lett.* **103** 057002
[24b] Williams A J, McQueen T M and Cava R J 2009 *Solid State Commun.* **149** 1507
[24c] Kotegawa H, Masaki S, Awai Y, Tou H, Mizuguchi Y and Takano Y 2009 *J. Phys. Soc. Japan* **78** 013709
[24d] Imai T, Ahilan K, Ning F L, McQueen T M and Cava R J 2009 *Phys. Rev. Lett.* **102** 177005
[25] Hsu F-C *et al* 2008 *Proc. Natl Acad. Sci. USA* **105** 14262
[26a] Margadonna S, Takabayashi Y, McDonald M T, Kasperkiewicz K, Mizuguchi Y, Takano Y, Fitch A N, Suard E and Prassides K 2008 *Chem. Commun.* 5607
[26b] Millican J N, Phelan D, Thomas E L, Leão J B and Carpenter E 2009 *Solid State Commun.* **149** 707
[26c] Medvedev S *et al* 2009 *Nat. Mater.* **8** 630
[27a] Lee C H, Ito T, Iyo A, Eisaki H, Kito H, Fernandez-Diaz M T, Kihou K, Matsuhata H, Braden M and Yamada K 2008 *J. Phys. Soc. Japan* **77** 083704
[27b] Rodgers J A, Penny G B S, Marcinkova A, Bos J-W G, Sokolov D A, Kusmartseva A, Huxley A D and Attfield J P 2009 *Phys. Rev.* B **80** 052508
[28] Nowik I and Felner I 2008 arXiv:0806.4078
Cimberle M R, Canepa F, Ferretti M, Martinelli A, Palenzona A, Siri A S, Tarantini C, Tropeano M and Ferdeghini C 2009 *J. Magn. Magn. Mater.* **321** 3024
[29] Coldea A I, Fletcher J D, Carrington A, Analytis J G, Bangura A F, Chu J-H, Erickson A S, Fisher I R, Hussey N E and McDonald R D 2008 *Phys. Rev. Lett.* **101** 216402
Coldea A I, Andrew C M J, Analytis J G, McDonald R D, Bangura A F, Chu J H, Fisher I R and Carrington A 2009 *Phys. Rev. Lett.* **103** 026404
Analytis J G, Andrew C M J, Coldea A I, McCollum A, Chu J H, McDonald R D, Fisher I R and Carrington A 2009 *Phys. Rev. Lett.* **103** 076401
[30] Fletcher J D, Serafin A, Malone L, Analytis J G, Chu J-H, Erickson A S, Fisher I R and Carrington A 2009 *Phys. Rev. Lett.* **102** 147001
[31] Subedi A, Zhang L, Singh D J and Du M H 2008 *Phys. Rev.* B **78** 134514
[32] Xia Y, Qian D, Wray L, Hsieh D, Chen G F, Luo J L, Wang N L and Hasan M Z 2009 *Phys. Rev. Lett.* **103** 037002
Nakayama K *et al* 2009 arXiv:0907.0763
[33] Welz D and Rosenberg M 1987 *J. Phys. C: Solid State Phys.* **20** 3911
[34] Bradley C J and Cracknell A P 1972 *The Mathematical Theory Of Symmetry in Solids* (Oxford: Clarendon)
[35] Vildosola V, Pourovskii L, Arita R, Biermann S and Georges A 2008 *Phys. Rev.* B **78** 064518
[36] Kimber S A J *et al* 2009 *Nat. Mater.* **8** 471
[37] Lu D H *et al* 2008 *Nature* **455** 81
[38] Kresin V Z and Wolf S A 2009 *Rev. Mod. Phys.* **81** 481
[39] Boeri L, Dolgov O V and Golubov A A 2008 *Phys. Rev. Lett.* **101** 026403
[40] Khasanov R, Luetkens H, Amato A, Klaus H-H, Ren Z-A, Yang J, Lu W and Zhao Z-X 2008 *Phys. Rev.* B **78** 092506
[41] Klingeler R, Leps N, Hellmann I, Popa A, Hess C, Kondrat A, Hamann-Borrero J, Behr G, Kataev V and Büchner B 2010 *Phys. Rev.* B **81** 024506
Wang X F, Wu T, Wu G, Chen H, Xie X L, Ying J J, Yan Y J, Liu R H and Chen X H 2009 *Phys. Rev. Lett.* **102** 117005

Yang J, Matsui M, Kawa M, Ohta H, Michioka C, Dong C,
  Wang H, Yuan H, Fang M and Yoshimura K 2009
  arXiv:0911.4758
[42] Halperin B I and Rice T M 1968 *Rev. Mod. Phys.* **40** 755
[43] Wilson J A, DiSalvo F J and Mahajan S 1975 *Adv. Phys.*
  24 117
[44] Wilson J A and Mahajan S 1977 *Commun. Phys.* **2** 23
  Wilson J A 1978 *Phys. Status Solidi* b **86** 11
[45] DiSalvo F J, Moncton D E and Waszczak J V 1976 *Phys.
  Rev.* B **14** 4321
[46] Withers R L and Wilson J A 1986 *J. Phys. C: Solid State
  Phys.* **19** 4809
[47] Freidberg R and Lee T D 1989 *Phys. Lett.* A **138** 423
  Freidberg R and Lee T D 1989 *Phys. Rev.* B **40** 6745
[48] Byczuk K and Vollhardt D 2009 *Ann. Phys.* **18** 622
[49a] Wilson J A 1988 *J. Phys. C: Solid State Phys.* **21** 2067
[49b] Wilson J A and Zahrir A 1997 *Rep. Prog. Phys.* **60** 941
[49c] Wilson J A 2004 *Phil. Mag.* **84** 2183
[49d] Wilson J A 2008 *J. Phys.: Condens. Matter* **20** 385210
[49e] Wilson J A 2009 *J. Phys.: Condens. Matter* **21** 245702
[50] Gooch M, Lv B, Tapp J H, Tang Z, Lorenz B, Guloy A M
  and Chu C W 2009 *Europhys. Lett.* **85** 27005
[51] Liu R H *et al* 2008 *Phys. Rev. Lett.* **101** 087001
  Hess C, Kondrat A, Narduzzo A, Hamann-Borrero J E,
  Klingeler R, Werner J, Behr G and Büchner B 2009
  Europhys. Lett. **87** 17005
[52] Bud'ko S L, Ni N and Canfield P C 2009 *Phys. Rev.* B **79**
  220516(R)
[53a] McQueen T M *et al* 2009 *Phys. Rev.* B **79** 014522
[53b] Song Y J, Hong J B, Min B H, Lee K J, Jung M H,
  Rhyee J-S and Yong S K 2010 arXiv:0911.2045v2
[53c] Kang N, Auban-Senzier P, Pasquier C R, Ren Z A, Yang Y,
  Che G C and Zhao Z X 2009 *New J. Phys.* **11** 025006
[54] Yoshida R *et al* 2009 *J. Phys. Soc. Japan* **78** 034708
[55] Carlo J P *et al* 2009 *Phys. Rev. Lett.* **102** 087001
[56] Grafe H-J *et al* 2008 *Phys. Rev. Lett.* **101** 047003
  Grafe H-J *et al* 2009 *New J. Phys.* **11** 035002
[57] Yashima M, Nishimura H, Mukuda H, Kitaoka Y,
  Miyazawa K, Shirage P M, Kiho K, Kito H, Eisaki H and
  Iyo A 2009 *J. Phys. Soc. Japan* **78** 103702
  Fukazawa H *et al* 2009 *J. Phys. Soc. Japan* **78** 033704
[58] Masaki S, Kotegawa H, Hara Y, Tou H, Murata K,
  Mizuguchi Y and Takano Y 2009 *J. Phys. Soc. Japan*
  78 063704
[59] Tatsumi K, Fujiwara N, Okada H, Takahashi H, Kamihara Y,
  Hirano M and Hosono H 2009 *J. Phys. Soc. Japan*
  78 023709
[60] Ishikado M *et al* 2009 *J. Phys. Soc. Japan* **78** 043705
[61] Zhao J *et al* 2008 *Nat. Mater.* **7** 953
[62] Christianson A D *et al* 2008 *Nature* **456** 930
[63] Inosov D S *et al* 2009 arXiv:0907.3632
[64] Zhao J, Regnault L-P, Zhang C, Wang M, Li Z, Zhou F,
  Zhao Z and Dai P 2009 arXiv:0908.0954
[65] Hwang J, Yang T, Timusk T, Sharapov S G, Carbotte J P,
  Bonn D A, Liang R and Hardy W N 2006 *Phys. Rev.* B
  73 014508
[66] Yang J, Hwang J, Schachinger E, Cabotte J P, Lobo R P S M,
  Colson D, Forget A and Timusk T 2009 *Phys. Rev. Lett.*
  102 027003
[67] Yang J, Hüvonen D, Nagel U, Rõõm T, Ni N, Canfield P C,
  Bud'ko S L, Carbotte J P and Timusk T 2009 *Phys. Rev.
  Lett.* **102** 187003
[68] Ding H *et al* 2008 *Europhys. Lett.* **83** 47001
[69] Carrington A, Meeson P J, Cooper J R, Balicas L,
  Hussey N E, Yelland E A, Lee S, Yamamoto A,
  Tajima S and Karpinski J 2003 *Phys. Rev. Lett.* **91** 037003
  Kortus J 2007 *Physica* C **456** 54
  Blumberg G, Mialitsin A, Dennis A, Zhigadlo N D and
  Karpinski J 2007 *Physica* C **456** 75
[70] Yi M *et al* 2009 *Phys. Rev.* B **80** 024515
[71] Xu Y-M *et al* 2009 arXiv:0905.4467
[72] Hicks C W, Lippman T M, Huber M E, Ren Z-A, Yang J,
  Zhao Z-X and Moler K A 2009 *J. Phys. Soc. Japan*
  78 013708
[73] Chubukov A V, Efremov D and Eremin I 2008 *Phys. Rev.* B
  78 134512
[74] Sologubenko A V, Jun J, Kazakov S M, Karpinski J and
  Ott H R 2002 *Phys. Rev.* B **66** 014504
[75] Boaknin E *et al* 2003 *Phys. Rev. Lett.* **90** 117003
[76] Baker P J, Giblin S R, Pratt F L, Liu R H, Wu G, Chen X H,
  Pitcher M J, Parker D R, Clarke S J and Blundell S J 2008
  arXiv:0811.2494 (sub*d* to N.J.P.)
[77] Mu G, Luo H, Wang Z, Shan L, Ren C and Wen H-H 2009
  Phys. Rev. B **79** 174501
[78] Mu G, Zhu X Y, Fang L, Shan L, Ren C and Wen H-H 2008
  Chin. Phys. Lett. **25** 2221
[79] Baumbach R E, Hamlin J J, Shu L, Zocco D A, Crisosto N M
  and Maple M B 2009 *New J. Phys.* **11** 025018
  Analytis J, Chu J-H, Erickson A S, Kucharczyk C,
  Seraphin A, Carrington A, Cox C, Kauzlarich S M,
  Hakon H and Fisher I R 2008 arXiv:0810.5368
[80] Qazilbash M M, Hamlin J J, Baumbach R E, Zhang L,
  Singh D J, Maple M B and Basov D N 2009 *Nat. Phys.*
  5 648
[81] Tajima S, Fudamoto Y, Kakeshita T, Gorshunov B,
  Železný V, Kojima K M, Dressel M and Uchida S 2005
  Phys. Rev. B **71** 094508
  Homes C C, Dordevic S V, Gu G D, Li Q, Valla T and
  Tranquada J M 2006 *Phys. Rev. Lett.* **96** 257002
[82] Cooper R A *et al* 2009 *Science* **323** 603
[83] Malone L, Fletcher J D, Serafin A, Carrington A,
  Zhigadlo N D, Bukowski Z, Katrych S and
  Karpinski J 2009 *Phys. Rev.* B **79** 140501(R)
[84] Khasanov R *et al* 2008 *Phys. Rev.* B **78** 220510(R)
[85] Gordon R T, Martin C, Kim H, Ni N, Tanatar M A,
  Schmalian J, Mazin I I, Bud'ko S L, Canfield P C and
  Prozorov R 2009 *Phys. Rev.* B **79** 100506(R)
  Martin C *et al* 2009 *Phys. Rev.* B **80** 020501
[86] Wilson J A 2006 *J. Phys.: Condens. Matter* **18** R69
  Wilson J A 2008 *J. Phys.: Condens. Matter* **20** 015215
[87] Canfield P C and Bud'ko S L 2010 arXiv:1002.0858
[88] Chen H *et al* 2008 arXiv:0807.3950
[89] Jia S, Williams A J, Stephens P W and Cava R J 2009
  arXiv:0909.2002
[90] Ning F, Ahilan K, Imai T, Sefat A S, Jin R, McGuire M A,
  Sales B C and Mandrus D 2009 *J. Phys. Soc. Japan*
  78 013711
[91] Kotegawa H, Sugawara H and Tou H 2009 *J. Phys. Soc.
  Japan* **78** 013709
  Matsubayashi K, Katayama N, Ohgushi K, Yamada A,
  Munakata K, Matsumoto T and Uwatoko Y 2009 *J. Phys.
  Soc. Japan* **78** 073706
[92] Jiang S, Xing H, Xuan G, Wang C, Ren Z, Feng C, Dai J,
  Xu Z and Cao G 2009 *J. Phys.: Condens. Matter*
  21 382203
[93] Hiramatsu H, Katase T, Kamiya T, Hirano M and
  Hosono H 2009 *Phys. Rev.* B **80** 052501
[94] Burrow J H, Maule C H, Strange P, Tothill J N and
  Wilson J A 1987 *J. Phys. C: Solid State Phys.* **20** 4115
[95] Ogino H, Matsumura Y, Katsura Y, Ushiyama K, Horii S,
  Kishio K and Shimoyama J 2009 *Supercond. Sci. Technol.*
  22 075008
[96a] Ogino H, Katsura Y, Horii S, Kishio K and
  Shimoyama J 2009 *Supercond. Sci. Technol.* **22** 085001
[96b] Xie Y L *et al* 2009 *Europhys. Lett.* **86** 57007
[97] Zhu X, Han F, Mu G, Cheng P, Shen B, Zeng B and
  Wen H-H 2009 *Phys. Rev.* B **79** 220512(R)
[98] Sato S, Ogino H, Kawaguchi N, Katsura Y, Kishio K,
  Shimoyama J, Kotegawa H and Tou H 2009
  arXiv:0912.1840
[99] Gotoh Y, Akimoto J, Goto M, Oosawa Y and Onoda M 1995
  J. Solid State Chem. **116** 61
[100] Tropeano M, Pallecchi I, Cimberle M R, Ferdeghini C,
  Lamura G, Vignolo M, Martinelli A, Palenzona A and
  Putti M 2009 arXiv:0912.0395
[101] Yuan H Q, Singleton J, Balakirev F F, Chen G F, Luo J L and
  Wang N L 2009 *Nature* **457** 565

[102] Kohama Y, Kamihara Y, Baily S A, Civale L, Riggs S C,
      Balakirev F F, Atake T, Jaime M, Hirano M and
      Hosono H 2009 *Phys. Rev.* B **79** 144527
[103] Riggs S C *et al* 2009 *J. Phys.: Condens. Matter* **21** 412201
[104] Kotegawa H, Kawazoe T, Tou H, Murata K, Ogino H,
      Kishio K and Shimoyama J 2009 arXiv:0908.1469
[105] Iida K, Hänisch J, Hühne R, Kurth F, Kidzun M, Haindl S,
      Werner J, Schultz L and Holzapfel B 2009 *Appl. Phys.
      Lett.* **95** 192501
[106a] Liu R H *et al* 2009 *Nature* **459** 64
[106b] Yanagisawa T, Odagiri K, Hase I, Yamaji K, Shirage P M,
      Tanaka Y, Iyo A and Eisaki H 2009 *J. Phys. Soc. Japan*
      78 094718
[107] Klingeler R, Wang L, Köhler U, Behr G, Hess C and
      Büchner B 2009 arXiv:0909.3998
[108] Pomjakushina E, Conder K, Pomjakushin V, Bendele M and
      Khasanov R 2009 *Phys. Rev.* B **80** 024517
[109] Wilson S D, Rotundu C R, Yamani Z, Valdivia P N,
      Freelon B, Bourret-Courchesne E and Birgeneau R J 2009
      arXiv:0910.0489
[110] Ryder J, Midgley P A, Exley R, Beynon R J, Yates D L,
      Afalfiz L and Wilson J A 1991 *Physica* C **173** 9
[111] LeTacon M *et al* 2009 *Phys. Rev.* B **80** 220504
[112] Fernandes R M, VanBebber L H, Bhattacharya S, Chandra P,
      Keppens V, Mandrus D, McGuire M A, Sales B C,
      Sefat A S and Schmalian J 2009 arXiv:0911.3084
[113] Haasen P 1978 *Physical Meturallurgy* (Cambridge:
      Cambridge University Press) chapter 5
      Sboychakov A O, Rakhmanov A L and Kugel K I 2009
      arXiv:0911.4401
[114a] Park J T *et al* 2009 *Phys. Rev. Lett.* **102** 117006
[114b] Inosov D S *et al* 2009 *Phys. Rev.* B **79** 224503
[115] Sanna S, De Renzi R, Lamura G, Ferdeghini C, Palenzona A,
      Putti M, Tropeano M and Shiroka T 2009 *Phys. Rev.* B
      80 052503
[116] McQueen T M, Williams A J, Stephens P W, Tao J, Zhu Y,
      Ksenofontov V, Casper F, Felser C and Cava R J 2009
      Phys. Rev. Lett. **103** 057002
[117] Nomura T, Kim S W, Kamihara Y, Hirano M, Sushko P V,
      Kato K, Takata M, Shluger A L and Hosono H 2008
      Supercond. Sci Technol. **21** 125028
[118] Zhang S J *et al* 2009 *Phys. Rev.* B **80** 014506
[119] Katayama N *et al* 2009 *Phys. Rev. Lett.* **103** 146405
[120] Withers R L, Hua G L, Welberry T R and Vincent R 1988
      J. Phys. C: Solid State Phys. **21** 309
[121] Wang M J, Luo J Y, Huang T W, Chang H H, Chen T K,
      Hsu F C, Wu C T, Wu P M, Chang A M and Wu M K
      2009 *Phys. Rev. Lett.* **103** 117002
[122] Horigane K, Hiraka H and Ohoyama K 2009 *J. Phys. Soc.
      Japan* **78** 074718
[123] Garbarino G, Sow A, Lejay P, Sulpice A, Toulemonde P,
      Mezouar M and Nuñez-Regueiro M 2009 *Europhys. Lett.*
      86 27001
[124] Li S, de la Cruz C, Huang Q, Chen G F, Xia T-L, Luo J L,
      Wang N L and Dai P 2009 *Phys. Rev.* B **80** 020504(R)
[125] Kogan V G, Martin C and Prozorov R 2009 *Phys. Rev.* B
      80 014507
[126] Khasanov R, Bendele M, Amato A, Conder K, Elender M,
      Keller H, Klaus H-H, Luetkens H, Pomjakushina E and
      Raselli A 2009 arXiv:0908.2734
[127] Weyeneth S *et al* 2009 arXiv:0911.5420
[128] Miyoshi K, Takaichi Y, Mutou E, Fujiwara K and
      Takeuchi J 2009 *J. Phys. Soc. Japan* **78** 093703
[129] Fernandes R M *et al* 2009 *Phys. Rev.* B **81** 140501(R)
      Pratt D K, Tian W, Kreyssig A, Zarestky J L, Nandi S, Ni N,
      Bud'ko S L, Canfield P C, Goldman A I and
      McQueeney R J 2009 *Phys. Rev. Lett.* **103** 087001
[130] Perucchi A *et al* 2009 arXiv:0907.3639
[131] Wilson J A 1991 *Physica* C **182** 1
[132] Schluter M. Lannoo M, Needels M, Baraff G A and
      Tomanek D 1992 *Phys. Rev. Lett.* **68** 526
[133] Mazin I I, Andersen O K, Jepsen O, Dolgov O V, Kortus J,
      Golubov A A, Kuz'menko A B and van der Marel D 2002
      Phys. Rev. Lett. **89** 107002
      Boeri L, Bachelet G B, Cappelluti E and Pietronero L 2003
      Supercond. Sci. Technol. **16** 143
[134] Lee S C, Satomi E, Kobayashi Y and Sato M 2010 *J. Phys.
      Soc. Japan* **79** 023702
      Brouet V *et al* 2010 arXiv:1002.4952
[135] Wilson J A 1978 *Phys. Status Solidi* b **86** 11
[136] Kusmartseva A F, Sipos B, Berger H, Forró L and
      Tutiš E 2009 *Phys. Rev. Lett.* **103** 236401
      Monney C *et al* 2009 arXiv:0911.0327
[137] Wilson J A 1978 *Bell Technical Memorandum* 78-1527-15
[138] Yamanaka S, Hotehama K and Kawaji H 1998 *Nature*
      392 580
[139] Wilson J A 1999 *Supercond. Sci. Technol.* **12** 649
[140] Kasahara Y, Kishiume T, Takano T, Kobayashi K,
      Matsuoka E, Onodera H, Kuroki K, Taguchi Y and
      Iwasa Y 2009 *Phys. Rev. Lett.* **103** 077004
[141] Valyanskaya T V and Stepanov G N 1993 *Solid State
      Commun.* **86** 723
[142] Struzhkin V V, Hemley R J, Mao H-K and Timofeev Y A
      1997 *Nature* **390** 382
[143] Pickard C J and Needs R J 2009 *Phys. Rev. Lett.* **102** 146401
      Marqués M, Ackland G J, Lundegaard L F, Stinton G,
      Nelmes R J, McMahon M I and Contreras-Garcia J 2009
      Phys. Rev. Lett. **103** 115501
      Katzke H and Toledano P 2007 *Phys. Rev.* B **75** 174103
[144] Struzhkin V V, Eremets M I, Gan W, Mao H-K and Mao R J
      2002 *Science* **298** 1213
[145] Yabuuchi T, Matsuoka T, Nakamoto Y and Shimizu K 2006
      J. Phys. Soc. Japan **75** 083703
      Fujihisa H, Nakamoto Y, Shimizu K, Yabuuchi T and
      Gotoh Y 2008 *Phys. Rev. Lett.* **101** 095503
      Yin Z P, Gygi F and Pickett W E 2009 *Phys. Rev.* B
      80 184515
[146] Kim J S *et al* 2009 *J. Phys.: Condens. Matter* **21** 342201